© 2016. Published by The Company of Biologists Ltd | Journal of Cell Science (2016) 129, 693-705 doi:10.1242/jcs.169011

RESEARCH ARTICLE

Loss of PPARγ in endothelial cells leads to impaired angiogenesis

Sanna Vattulainen-Collanus[1], Oyediran Akinrinade[1,2], Molong Li[3,4], Minna Koskenvuo[5], Caiyun Grace Li[6], Shailaja P. Rao[6], Vinicio de Jesus Perez[7], Ke Yuan[7], Hirofumi Sawada[6,8], Juha W. Koskenvuo[4,9], Cristina Alvira[6], Marlene Rabinovitch[6] and Tero-Pekka Alastalo[1,*]

ABSTRACT

Tie2-promoter-mediated loss of peroxisome proliferator-activated receptor gamma (PPARγ, also known as PPARG) in mice leads to osteopetrosis and pulmonary arterial hypertension. Vascular disease is associated with loss of PPARγ in pulmonary microvascular endothelial cells (PMVEC); we evaluated the role of PPARγ in PMVEC functions, such as angiogenesis and migration. The role of PPARγ in angiogenesis was evaluated in *Tie2CrePPARγ$^{flox/flox}$* and wild-type mice, and in mouse and human PMVECs. RNA sequencing and bioinformatic approaches were utilized to reveal angiogenesis-associated targets for PPARγ. *Tie2CrePPARγ$^{flox/flox}$* mice showed an impaired angiogenic capacity. Analysis of endothelial progenitor-like cells using bone marrow transplantation combined with evaluation of isolated PMVECs revealed that loss of PPARγ attenuates the migration and angiogenic capacity of mature PMVECs. *PPARγ*-deficient human PMVECs showed a similar migration defect in culture. Bioinformatic and experimental analyses newly revealed *E2F1* as a target of PPARγ in the regulation of PMVEC migration. Disruption of the PPARγ–E2F1 axis was associated with a dysregulated Wnt pathway related to the GSK3B interacting protein (GSKIP). In conclusion, PPARγ plays an important role in sustaining angiogenic potential in mature PMVECs through E2F1-mediated gene regulation.

KEY WORDS: Endothelial cell, Angiogenesis, PPARγ, E2F1, GSKIP, Wnt signaling, Pulmonary hypertension, Osteopetrosis

INTRODUCTION

Angiogenesis, in which new capillaries are formed from a pre-existing vascular network, requires a complex interplay between growth signals. When this sensitive balance is disturbed, abnormalities in blood vessel growth occur. This is observed in many diseases including cancer, cardiopulmonary disorders and diabetes (Adair and Montani, 2010; Adams and Alitalo, 2007; Delgado et al., 2011). Endothelial cell migration, an essential component of angiogenesis, is directionally regulated by chemotactic, haptotactic, and mechanotactic stimuli and involves degradation of the extracellular matrix to allow movement of the endothelial cells. This process requires the activation of several signaling pathways that modulate cytoskeletal remodeling (Adams and Alitalo, 2007; Gerhardt, 2008; Lamalice et al., 2007). Growth factors, such as vascular endothelial growth factor (VEGF) and bone morphogenetic proteins (BMPs) among others, drive these angiogenic events (David et al., 2009; Gerhardt, 2008).

Peroxisome-proliferator-activated receptors (PPARs) are ligand-inducible nuclear transcription factors that are best known for their involvement in lipid and glucose homeostasis. PPARs also regulate inflammation and proliferation. There are three known PPAR isotypes: PPARα, PPARβ/δ, and PPARγ (Calkin and Thomas, 2008). Although PPARs exhibit tissue-specific patterns of expression, all are expressed in endothelial cells. PPAR-mediated regulation of vascular homeostasis has been extensively studied but the exact role of each PPAR isotype in angiogenesis is poorly understood. The lack of consensus about the angiogenic profile of specific PPARs seems to have arisen because of the differential effects of PPARs in various tissues and pathological states, and the usage of synthetic ligands that have pleiotropic effects (Calkin and Thomas, 2008; Desouza et al., 2009). However, there is general agreement that PPARs play a role in endothelial cell homeostasis (Biscetti et al., 2008; Bishop-Bailey, 2011; Desouza et al., 2009). To our knowledge, the use of transgenic animal models to study the role of PPARs in angiogenesis has been limited to the study of PPARβ/δ-deficient mice (Piqueras et al., 2007), showing an attenuated angiogenic capacity in matrigel plug assays.

Several transgenic animal models have been established to study the role of PPARγ (also known as PPARG) in other physiological processes. One such model is the *Tie2CrePPARγ$^{flox/flox}$* mouse, lacking functional PPARγ in endothelial cells and osteoclasts (Wan et al., 2007). This mouse has several pathogenic phenotypes, including osteopetrosis with extramedullary hematopoiesis but normal levels of circulating red and white blood cells. Furthermore, these *Tie2CrePPARγ$^{flox/flox}$* mice showed baseline pulmonary arterial hypertension (PAH) and impaired reversal of PAH after chronic hypoxia (Guignabert et al., 2009). The pathobiology underlying the pulmonary endothelial cell dysfunction was related to disrupted BMP receptor 2 (BMPR2)-mediated β-catenin interaction with PPARγ, required for pulmonary endothelial cell survival and proliferation (Alastalo et al., 2011; de Jesus Perez et al., 2009). This interaction demonstrated an intersection between the BMP and Wnt signaling pathways, and disruption of this interaction attenuated pulmonary endothelial cell survival and proliferation. Global chromatin immunoprecipitation on chip (ChIP-chip) identified *apelin* as a crucial target gene of the PPARγ–β-catenin complex in the regulation of pulmonary endothelial cell homeostasis. Furthermore, *apelin* expression was attenuated in the *Tie2CrePPARγ$^{flox/flox}$* mice, and in mice treated with apelin, PAH and abnormal pulmonary vascular remodeling was reversed (Alastalo et al., 2011).

[1]Children's Hospital Helsinki, Pediatric Cardiology, University of Helsinki and Helsinki University Central Hospital, Helsinki 00290, Finland. [2]Institute of Biomedicine, University of Helsinki, Helsinki 00290, Finland. [3]The Johns Hopkins University School of Medicine, Baltimore, MD 21205, USA. [4]Research Center of Applied and Preventive Cardiovascular Medicine, University of Turku, Turku 20520, Finland. [5]Children's Hospital Helsinki, Division of Hematology-Oncology and Stem Cell Transplantation, University of Helsinki and Helsinki University Central Hospital, 00290 Helsinki, Finland. [6]Department of Pediatrics, Wall Center for Pulmonary Vascular Disease, Cardiovascular Institute Stanford University, Stanford, CA 94305, USA. [7]Division of Pulmonary and Critical Care Medicine, Stanford University, Stanford, CA 94305, USA. [8]Department of Pediatrics, Mie University Graduate School of Medicine, Mie 5148507, Japan. [9]Department of Clinical Physiology and Nuclear Medicine, HUS Medical Imaging Center, Helsinki University Central Hospital and University of Helsinki, 00290 Helsinki, Finland.

*Author for correspondence (tero-pekka.alastalo@helsinki.fi)

Received 19 January 2015; Accepted 30 December 2015

Journal of Cell Science

Journal of Cell Science (2016) 129, 693-705 doi:10.1242/jcs.169011

Here, we show that the loss of PPARγ leads to an attenuated angiogenic response. Using RNA sequencing and bioinformatic approaches together with cultured pulmonary microvascular endothelial cells (PMVEC) and an experimental animal model, we showed that PPARγ plays an important role in sustaining angiogenic potential in mature PMVECs through E2F1. Disruption of the PPARγ–E2F1 axis was associated with dysregulated Wnt signaling through genes such as GSK3B interacting protein (*GSKIP*).

RESULTS

To study the role of PPARγ in angiogenesis we assessed the degree of neovascularization in matrigel plugs in wild-type (WT) and *Tie2CrePPARγ*$^{flox/flox}$ mice treated with and without BMP2 stimulation. Whereas BMP2-stimulated plugs in WT mice showed a sevenfold increase in vessel number compared with those treated with vehicle, BMP2 did not stimulate an angiogenic response in the plugs in *Tie2CrePPARγ*$^{flox/flox}$ mice (Fig. 1A,B; Fig. S1A). This suggests that loss of angiogenic response in *Tie2CrePPARγ*$^{flox/flox}$ mice results from the loss of PPARγ in cells expressing Tie2 (also known as Tek), including endothelial cells (Tang et al., 2010). As the levels of circulating endothelial progenitor-like cells (EPCs) are considered a determinant of angiogenic capacity (Ciarrocchi et al., 2007; Shaked et al., 2005; Urbich and Dimmeler, 2004), we investigated whether the reduced angiogenic capacity of *Tie2CrePPARγ*$^{flox/flox}$ mice was related to changes in circulating EPC-like cells. Whereas defining true EPCs remains under constant discussion (Richardson and Yoder, 2011; Yoder, 2009), we assessed the levels of EPC-like cells from blood, spleen and bone marrow of WT and *Tie2CrePPARγ*$^{flox/flox}$ mice by FACS analysis using CD34 and VEGFR2 (also known as KDR) as markers (Asahara et al., 1999; Chakroborty et al., 2008; Madeddu et al., 2004; Schuch et al., 2003; Shmilovich et al., 2007). As the changes in CD34$^+$/VEGFR2$^+$ levels in the bone marrow and spleen were similar in samples obtained with or without prior CD45 selection, the CD45$^-$ population was not excluded in the blood. In the blood and spleen, levels of CD34$^+$/VEGFR2$^+$ cells were significantly reduced in *Tie2CrePPARγ*$^{flox/flox}$ mice (Fig. 1C,D). In the bone marrow, levels of CD34$^+$/VEGFR2$^+$ cells were threefold higher in *Tie2CrePPARγ*$^{flox/flox}$ mice versus WT mice (Fig. 1E), suggesting that the *Tie2CrePPARγ*$^{flox/flox}$ mice have a defect in the mobilization of CD34$^+$/VEGFR2$^+$ cells from the bone marrow.

To determine whether the impaired angiogenic capacity observed in *Tie2CrePPARγ*$^{flox/flox}$ mice was related to the reduction in circulating CD34$^+$/VEGFR2$^+$ cells, bone marrow transplant experiments were performed. The transplantation of lethally irradiated WT mice with bone marrow isolated from *Tie2CrePPARγ*$^{flox/flox}$ mice induced the accumulation of CD34$^+$/VEGFR2$^+$ cells in the bone marrow, and decreased levels of these cells in circulation and spleen (compare WT results in Fig. 1F–H with Fig. 1C–E). This phenotypic switch between the two mouse genotypes confirmed the association of Tie2-mediated PPARγ deficiency with decreased levels of circulating CD34$^+$/VEGFR2$^+$ cells.

Next, we determined whether the bone marrow from WT mice could rescue the attenuated angiogenic capacity of *Tie2CrePPARγ*$^{flox/flox}$ mice. Whereas WT bone marrow transplantation effectively increased the levels of circulating CD34$^+$/VEGFR2$^+$ cells in *Tie2CrePPARγ*$^{flox/flox}$ mice (compare KO results in Fig. 1F–H with Fig. 1C–E), it did not rescue the angiogenic defect (compare Fig. 1I with Fig. 1B). This suggests that *PPARγ* deficiency in resident, mature PMVECs might influence the angiogenic capacity to a greater degree than the loss

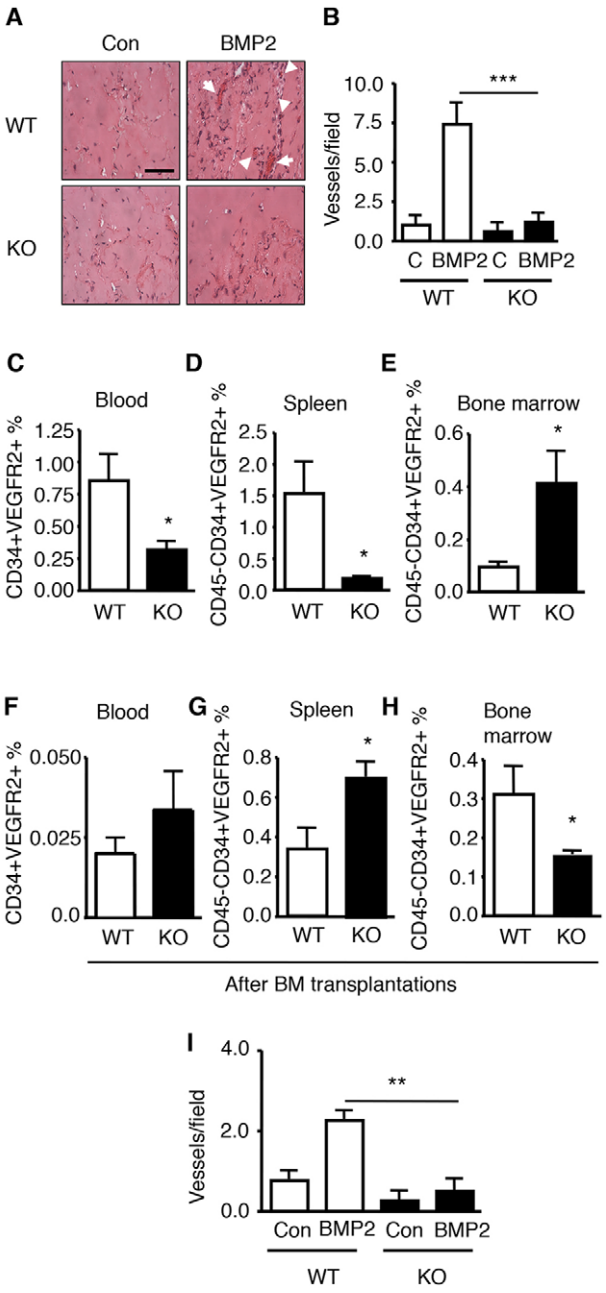

Fig. 1. Loss of PPARγ attenuates angiogenesis and impairs EPC-like cell mobilization from the bone marrow. (A) *In vivo* angiogenesis assay with subcutaneously placed matrigel plugs in wild-type (WT) and *TIE2CrePPARγ*$^{flox/flox}$ (KO) mice. Arrows indicate blood vessels in matrigel plugs stimulated with vehicle (H_2O; Con) or BMP2 (10 ng/ml). Scale bar: 25 mm. (B) Number of vessels per field (20× magnification) was used for quantifying vessels. 'C' refers to control conditions. (C–E) Percentage of CD34$^+$/VEGFR2$^+$ cells in gated live cell population from blood (C), and CD34$^+$/VEGFR2$^+$/CD45$^-$ live cell population from (D) spleen and (E) bone marrow of WT and KO mice was analyzed using flow cytometry. (F–H) Cross-transplantation of bone marrow between KO and WT mice rescued the cell mobilization defect of the CD34$^+$/VEGFR2$^+$ live cell population in samples from blood (F) and CD34$^+$/VEGFR2$^+$/CD45$^-$ cells in live cell population in samples from (G) spleen and (H) bone marrow in KO mice. (I) *In vivo* angiogenesis in WT and KO mice was analyzed by matrigel plug assay after bone marrow (BM) transplantation. The angiogenic defect in KO mice was not rescued after bone marrow transplantation from WT mice. Error bars represent mean±s.e.m. from six matrigel plugs from three separate mice in B and I and from 3–5 mice per group in C–H. **P*<0.05, ***P*<0.01, ****P*<0.001 versus respective control; one-way ANOVA with Bonferroni's multiple comparison tests in B,I; unpaired two-tailed *t*-test in C–H.

Journal of Cell Science (2016) 129, 693-705 doi:10.1242/jcs.169011

of PPARγ from bone-marrow-derived circulating cells, such as EPCs. Our functional studies with PMVECs showed that BMP2- and VEGF-stimulated tube formation and migration were attenuated in PMVECs isolated from *Tie2CrePPARγ*$^{flox/flox}$ mice (Fig. 2A–C). Given that the attenuated angiogenic capacity was not restricted to BMP signaling, VEGF was used as the angiogenic stimulus in the subsequent cell culture studies. Downregulation of PPARγ in human PMVECs using siRNA methods was validated by qPCR and western immunoblotting (Fig. S1B,C). Loss of PPARγ led to a migration defect in human primary PMVECs (Fig. 2D) similar to that observed in the *Tie2CrePPARγ*$^{flox/flox}$ mice (Fig. 2C), confirming that *PPARγ* deficiency attenuates migration both in mouse and human PMVECs.

As angiogenesis is also dependent on proliferation and survival, we next studied whether loss of PPARγ affected proliferation and survival capacity of human PMVECs. The cell count experiments and MTT proliferation assays revealed that *PPARγ*-silenced human PMVECs lost their proliferation capacity after serum-stimulation (Fig. S1D,E). Furthermore, *PPARγ*-silenced human PMVECs showed significantly lower survival capacity and increased caspase 3/7 activity under stress conditions (Fig. S1F,G). However, PMVECs isolated from *Tie2CrePPARγ*$^{flox/flox}$ mice did not lose their ability to proliferate and survive under stress conditions *in vitro* (data not shown), suggesting that chronic suppression of PPARγ in mouse PMVECs is partially compensated when compared with acute suppression in human PMVECs. Given that VEGFR2 plays an important role in vascular endothelial cell biology and has been shown to be a target of ligand-activated PPARγ (Kim et al., 2011), we investigated whether VEGF–VEGFR2 signaling was altered by loss of PPARγ in human and murine PMVECs. Based on our results, neither VEGFR2 protein expression nor VEGFR2 phosphorylation differed between normal PMVECs and *PPARγ*-silenced human PMVECs or murine PMVECs from the *TIE2CrePPARγ*$^{flox/flox}$ mice (Fig. S1H,I). This suggests that loss of PPARγ suppresses angiogenic pathways other than VEGF–VEGFR2-mediated signaling.

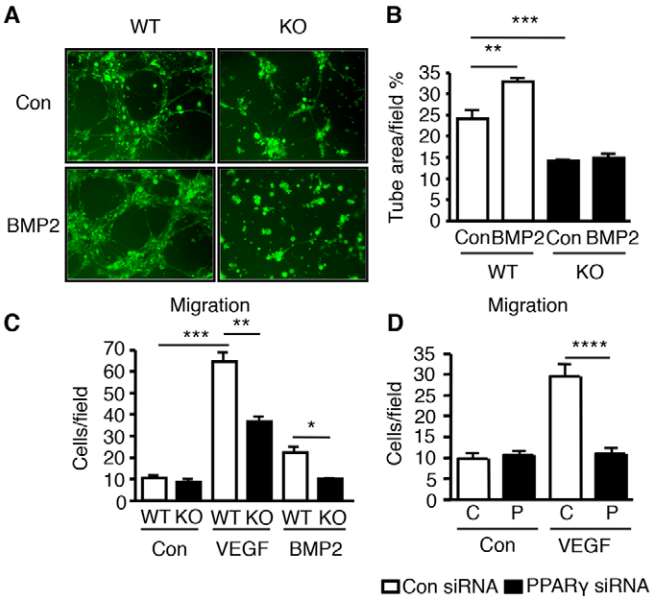

Fig. 2. Loss of PPARγ in mature endothelial cells attenuates the angiogenic response. (A) *In vitro* tube-formation with isolated PMVEC from wild-type (WT) and *TIE2CrePPARγ*$^{flox/flox}$ (KO) mice. Fluorescence microscopy was used to detect calcein-incorporated live cells and their tube structures after 16 h on matrigel, when treated with vehicle (H_2O; Con) and BMP2 (10 ng/ml). (B) Tube formation was quantified by tube area per total field area (10× magnification) from three different fields per experiment. (C) Migration assay with PMVECs isolated from WT and KO mice and stimulated with vehicle (H_2O; Con), VEGF (50 ng/ml) and BMP2 (10 ng/ml) for 6 h. (D) Migration assay with Non-target ('C') and PPARγ ('P') siRNA-transfected human PMVECs stimulated with vehicle (H_2O; Con) and VEGF (50 ng/ml). The cells were counted from three different fields (20× magnification) at the center of each well to quantify the number of migrated cells in C and D. Error bars represent mean ±s.e.m. from four separate experiments in B and from three separate experiments in C,D. ***P*<0.01, ****P*<0.001, **** *P*<0.0001 versus respective control; one-way ANOVA with Bonferroni's multiple comparison tests.

Previously, we have identified apelin as a downstream target of BMP2-mediated signaling through PPARγ–β-catenin-mediated transcription (Alastalo et al., 2011). Consistent with this, Kasai et al. (2008) demonstrated that *apelin*-deficient mice exhibit a decreased angiogenic capacity. Having demonstrated that *apelin* expression is significantly decreased in PMVECs of *Tie2CrePPARγ*$^{flox/flox}$ mice and that apelin treatment can reverse pulmonary hypertension in these animals, we repeated the matrigel plug assays adding apelin with and without BMP2. In WT mice, BMP2 increased vessel formation and a modest further increase was observed when apelin was also added. In *Tie2CrePPARγ*$^{flox/flox}$ mice, apelin had a synergistic effect on BMP2-mediated angiogenesis, increasing vessel formation to a greater degree than either apelin or BMP2 treatment alone (Fig. 3A). A similar synergistic response was evident in migration assays performed with *PPARγ*-silenced human PMVECs. They also showed significantly lower *apelin* expression when compared with control PMVECs (data not show). This was also seen in PMVECs from *Tie2CrePPARγ*$^{flox/flox}$ versus control mice (Alastalo et al., 2011). We observed that migration was significantly increased in control human PMVECs after stimulation with VEGF, apelin, or both in combination. In *PPARγ*-depleted PMVECs, the attenuated VEGF response was partly restored by apelin co-treatment (Fig. 3B). These results suggest that apelin can partially restore the angiogenic capacity of *PPARγ*-deficient PMVECs both in mouse and human.

To better understand the full nature of the defect associated with loss of PPARγ in human PMVECs, we applied RNA sequencing to reveal global gene expression changes associated with *PPARγ* deficiency (Table S1A,B). In order to identify direct targets of PPARγ in pulmonary endothelial cells, we compared our RNA sequencing data with our previous PPARγ ChIP-chip analyses also carried out in pulmonary endothelial cells (Alastalo et al., 2011). The ChIP-chip dataset consisted of genes that showed promoter co-occupancy of both PPARγ and β-catenin (also known as CTNNB1 in human), and were significantly dysregulated upon attenuation of BMPR2 and β-catenin. These analyses revealed that *E2F1* is a novel target of PPARγ. The expression of *E2F1* mRNA was significantly downregulated in the RNA sequencing dataset after loss of PPARγ (Table S1B), and there was marked PPARγ occupancy on the *E2F1* promoter in our ChIP-chip dataset (Alastalo et al., 2011). The RNA sequencing result was confirmed by analyzing the mRNA level by qPCR and by determining significant downregulation of E2F1 protein after suppression of PPARγ in human PMVECs (Fig. 4A,B). There was also significant suppression of E2F1 protein in mouse PMVECs isolated from *Tie2CrePPARγ*$^{flox/flox}$ mice (Fig. 4C), confirming the linkage between PPARγ and E2F1 expression. Next, we confirmed the previous ChIP-chip result by performing ChIP analysis using the specific portion of the promoter identified as a putative PPARγ binding site by ChIP-chip (nucleotides −578 to +170). ChIP oligonucleotides were designed to overlap the putative PPARγ binding site in the promoter (nucleotides −103 and +170)

Journal of Cell Science (2016) 129, 693-705 doi:10.1242/jcs.169011

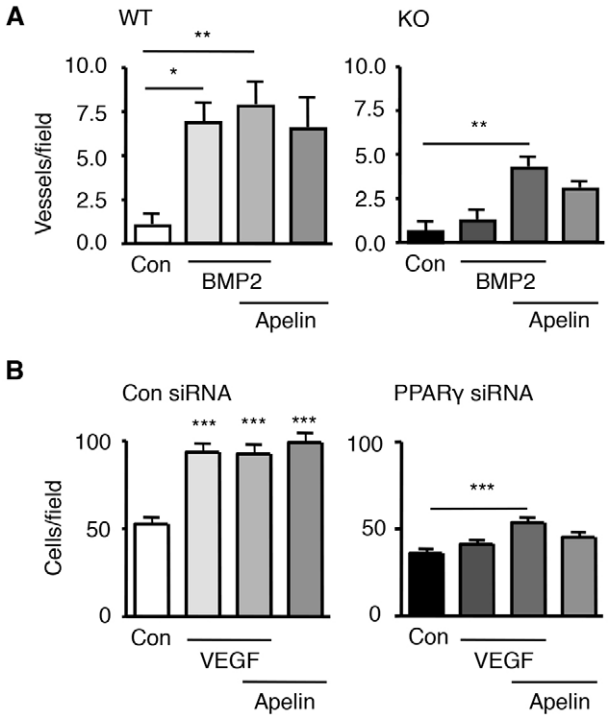

Fig. 3. Apelin can partially restore angiogenic defect both *in vivo* and *in vitro* after loss of PPARγ. (A) *In vivo* angiogenesis capacity was analyzed by matrigel plug assay. Matrigel plugs were placed subcutaneously into wild-type (WT) and *Tie2CrePPARγ*$^{flox/flox}$ (KO) mice. The number of blood vessels from matrigel plugs treated with vehicle (H_2O; Con), BMP2 (10 ng/ml), apelin (100 nM), and combination of BMP2 and apelin was counted. (B) Migration assay with human PMVEC treated with either Non-target siRNAs (Con) or with PPARγ-siRNA. Cells were stimulated with vehicle (H_2O; Con), VEGF (50 ng/ml), apelin (100 nM), and combination of VEGF and apelin. Error bars represent mean±s.e.m. from six matrigel plugs from three separate mice per group in A and from three separate experiments in B. *P<0.05, **P<0.01, ***P<0.001 versus respective control; one-way ANOVA with Bonferroni's multiple comparison tests.

(Alastalo et al., 2011), and extended upstream from the transcription start site. The ChIP analysis demonstrated that PPARγ is able to occupy this area of the *E2F1* promoter (Fig. S2A,B), suggesting that PPARγ could be an important transcriptional regulator of *E2F1*. In pre-adipocytes and brain cancer cells, E2F1 induces *PPARγ* expression (Bhatia et al., 2012; Fajas et al., 2002). To show the importance of PPARγ-mediated E2F1 expression in the phenotype observed, we reduced E2F1 using siRNA and confirmed downregulation by qPCR and western immunoblotting (Fig. S2C, D). *E2F1*-silenced human PMVECs showed attenuated migratory capacity (Fig. 4D). Interestingly, loss of E2FI in PMVECs did not alter levels of PPARγ expression (data not shown).

To further identify signaling networks and pathways that could be disrupted by loss of PPARγ and associated attenuation of E2F1, we performed gene ontology analysis on the human RNA sequencing dataset that we generated and this revealed significant enrichment of genes associated with cell cycle control (Table S2) and several pathways associated with cancer (Table S3), including p53, focal adhesion, apoptosis, TGF-β, and Wnt pathways. The expression of classical PPARγ target genes, such as *FABP4*, *CD36*, *CYP27A1*, *SORBS1*, *PCK2*, *MMP1* and *ACADM*, were also altered by *PPARγ*-knockdown. From the cancer-associated pathways, proteins within the Wnt signaling pathway were chosen as candidates for further functional studies (Table S4); the rationale being that we have previously identified and reported a PPARγ–β-catenin transcription factor complex downstream of BMPR2 signaling that is important in angiogenesis (Alastalo et al., 2011; de Jesus Perez et al., 2009), and Wnt signaling per se modulates cell migration and angiogenesis, and together with VEGF, is necessary for normal vascular development (Dejana, 2010; Goodwin and D'Amore, 2002; Zhang et al., 2001).

We used qPCR to validate expression of three Wnt pathway genes that were altered by loss of PPARγ: increased expression of *neucrin* (also known as *DRAXIN*), reduced expression of osteopetrosis associated transmembrane protein 1 (*OSTM1*) and *GSKIP* (Fig. S3). *neucrin* encodes a secreted protein within the Wnt signaling pathway that inhibits the stabilization of cytoplasmic β-catenin. Neucrin also appears to directly decrease cell migration (Miyake et al., 2009; Su et al., 2009). *OSTM1* encodes a type 1 transmembrane protein, which is localized in intracellular vesicles. OSTM1 enhances Wnt signaling by regulating β-catenin–Lef1 interaction and, when downregulated, suppresses the Wnt–β-catenin pathway (Feigin and Malbon, 2008). GSKIP is known to promote cell-cycle progression in neuronal cells by increasing the nuclear accumulation of β-catenin by inactivating GSK3β (also known as GSK3B) (Chou et al., 2006; Lin et al., 2009). These three genes were not detected in our previous PPARγ ChIP-chip dataset as direct targets of PPARγ (Alastalo et al., 2011). Furthermore, *in silico* promoter analysis of the *neucrin*, *OSTM1*, and *GSKIP* genes did not reveal any canonical PPARγ response elements (PPRE). Interestingly, the *GSKIP* promoter harbored an E2F1 binding site (Table S5), suggesting it could be a direct target of the PPARγ–E2F1 axis.

We pursued additional experiments centered on *GSKIP*. In the *PPARγ*-silenced human PMVECs, GSKIP protein and mRNA expression were significantly downregulated (Fig. 5A; Fig. S3). We hypothesized that attenuated expression of GSKIP would suppress the Wnt–β-catenin pathway by increasing GSK3β-mediated degradation of β-catenin. We confirmed that *PPARγ*-silenced human PMVECs contained significantly less of the inactive phosphorylated form of GSK3β (Ser9) than in control PMVECs, meaning that GSK3β was in the active form in these PPARγ-silenced PMVECs (Fig. 5B). Furthermore, both cytoplasmic and nuclear levels of β-catenin were decreased in *PPARγ*-silenced PMVECs (Fig. 5C,D). Interestingly, GSKIP expression was also significantly suppressed after loss of E2F1, and consequently the levels of active GSK3β were increased, leading to downregulation of β-catenin (Fig. 5E–G). To confirm the biological significance of PPARγ–E2F1-axis-mediated suppression of GSKIP and the Wnt–β-catenin pathway, we demonstrated partial rescue of the migratory defect associated with *PPARγ* or *E2F1* deficiency by BIO-Acetoxime; 6-Bromoindirubin-3′-acetoxime (BIA)- and LiCl-mediated inhibition of GSK3β (Fig. 6A–C; Fig. S4A–C). We further hypothesized that loss of GSKIP in human PMVECs leads to an angiogenic defect, similar to that seen in *PPARγ*-deficient PMVECs (Fig. 2A,B). First, we validated that GSKIP expression was effectively downregulated in human PMVECs after GSKIP siRNA transfections using qPCR and western immunoblotting (Fig. 7A,B). As hypothesized, *GSKIP*-silenced human PMVECs showed significantly impaired angiogenesis at baseline and following VEGF-stimulation when compared with control PMVECs (Fig. 7C,D). We then evaluated the expression level of GSKIP in PMVECs isolated from *Tie2CrePPARγ*$^{flox/flox}$ mice. In contrast to human PMVECs with loss of PPARγ by siRNA, *PPARγ*-deficient mouse cells showed a threefold elevation of GSKIP protein (Fig. 7E), suggesting the cells had adopted a compensatory

Journal of Cell Science (2016) 129, 693-705 doi:10.1242/jcs.169011

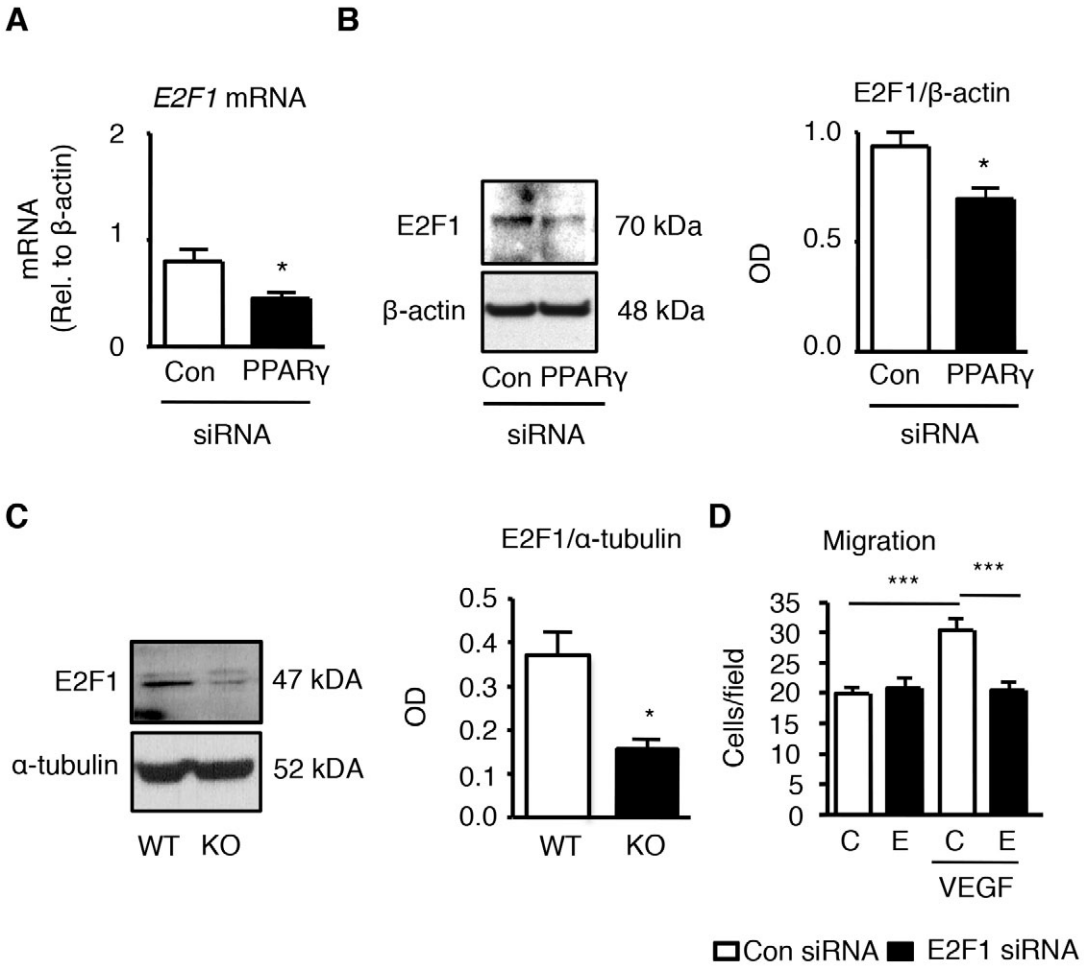

Fig. 4. Downregulation of PPARγ leads to a significant attenuation of E2F1. (A,B) Analysis of (A) *E2F1* mRNA expression (B) E2F1 protein expression in human PMVEC transfected with Non-target (Con) and PPARγ siRNAs. (C) E2F1 expression in wild-type (WT) and *Tie2CrePPARγ*$^{flox/flox}$ (KO) mice. Densitometry analysis was used to quantify the amount of protein per sample in B,C. (D) Migration assay in human PMVECs transfected with Non-target ('C') and E2F1 ('E') siRNA, stimulated with vehicle (H_2O; Con) and VEGF (50 ng/ml) for 6 h. Error bars represent mean±s.e.m. from three separate experiments. **P*<0.05, ****P*<0.001 versus respective control; unpaired two-tailed *t*-test in A–C; one-way ANOVA with Bonferroni's multiple comparison tests in D.

mechanism to cope with the attenuated PPARγ–E2F1 axis. In line with this, we observed similar expression of β-catenin between WT and *Tie2CrePPARγ*$^{flox/flox}$ mice (Fig. 7F). Interestingly, these mouse PMVECs have a significantly milder phenotype, normal survival and proliferation in *in vitro* assays, compared with human PMVEC with PPARγ-depletion.

DISCUSSION

Here, we describe a newly discovered mechanism by which PPARγ can regulate endothelial cell homeostasis and angiogenesis. We demonstrate in mouse and human PMVECs that loss of PPARγ leads to attenuated migration. Our data demonstrate that a previously described PPARγ target gene *apelin* can partially rescue the attenuated migratory capacity associated with *PPARγ* deficiency. Using RNA sequencing and previously published PPARγ ChIP-chip data, we identified *E2F1* as a novel downstream target of PPARγ that is important in the migratory capacity of PMVECs. We also demonstrate in human PMVECs that loss of the PPARγ–E2F1 axis suppresses the Wnt–β-catenin pathway (Fig. 8).

Although it is unclear if other PPAR nuclear receptors influence the angiogenic capacity of PMVECs in a manner similar to PPARγ, it has been reported that *PPARβ*-deficient mice show attenuated neovascularization (Müller-Brüsselbach et al., 2007). In addition to regulation of endothelial cell homeostasis, PPARγ has been reported as an important regulator of differentiation- and maturation-related processes. For example, PPARγ is a master regulator of adipocyte differentiation and adipogenesis. Interestingly, BMP2 is also a potent inducer of adipogenesis, although the direct link between PPARγ activation and BMP2 was not described (Zehentner et al., 2000). PPARγ has also been linked to other differentiation-related processes, including placental and cardiac development during early embryogenesis (Barak et al., 1999), postnatal lung maturation (Simon et al., 2006), and osteoclast differentiation (Wan et al., 2007). These observations suggest that PPARγ can modulate signaling pathways important in terminal differentiation of various cell types.

Previous studies using synthetic PPARγ ligands have often produced contradictory results regarding the role of PPARγ in angiogenesis (Desouza et al., 2009; Duan et al., 2008; Murata et al., 2000). We have observed that some synthetic ligands can serve as inhibitors of PPARγ rather than activators because they disrupt interactions with other transcription factors. Moreover, the role of PPARγ might vary depending on the pathological state of the cell or tissue being examined. Supporting our work is a recent study in which attenuation of PPARγ expression was shown to lead to decreased tube formation, and explain pulmonary arterial

Journal of Cell Science (2016) 129, 693-705 doi:10.1242/jcs.169011

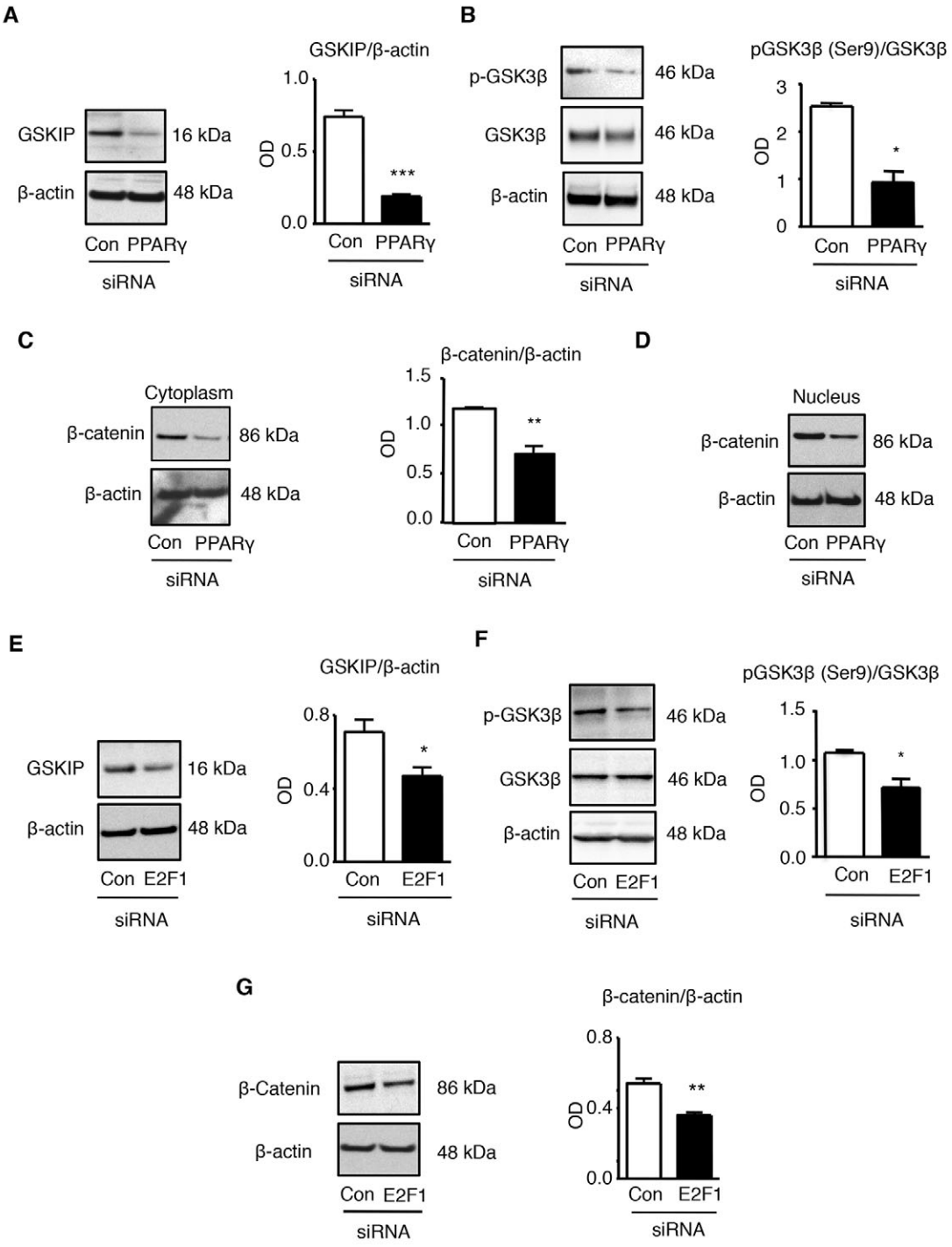

Fig. 5. Loss of PPARγ leads to similar dysregulation of Wnt signaling as downregulation of E2F1. Human PMVECs were transfected with Non-target, PPARγ, or E2F1 siRNAs. Samples were collected 48 h after initiation of transfections. (A,B) Protein expression levels of (A) GSKIP and (B) phosphorylated GSK3β (Ser9), in PMVECs transfected with Non-target (Con) and PPARγ siRNA. (C,D) β-catenin protein expression in PMVECs transfected with Non-target (Con) and PPARγ siRNA measured in the (C) cytoplasm and (D) nucleus. (E–G) Protein expression levels of (E) GSKIP, (F) phosphorylated GSK3β (Ser9), and (G) β-catenin, in PMVECs transfected with Non-target (Con) and E2F1 siRNA. Densitometry analysis was used to quantify the amount of protein per sample in A–C,E–G. Error bars represent mean±s.e.m. from three separate experiments. **P*<0.05, ***P*<0.01, ****P*<0.001 versus respective control; unpaired two-tailed *t*-test.

endothelial cell dysfunction and impaired angiogenesis seen in newborns with persistent pulmonary hypertension (Wolf et al., 2014). These reports are in line with our findings that Tie2-mediated loss of PPARγ in endothelial cells not only attenuates angiogenic capacity but also causes spontaneous development of pulmonary vascular disease (Guignabert et al., 2009). Furthermore, *Tie2CrePPARγ*$^{flox/flox}$ mice are more susceptible to systemic hypertension under a high-fat diet (Nicol et al., 2005). The migratory defect and dysregulation of crucial signaling pathways that we identified are likely to underlie part of the endothelial cell dysfunction in previously observed vascular diseases associated with *PPARγ* deficiency.

Journal of Cell Science (2016) 129, 693-705 doi:10.1242/jcs.169011

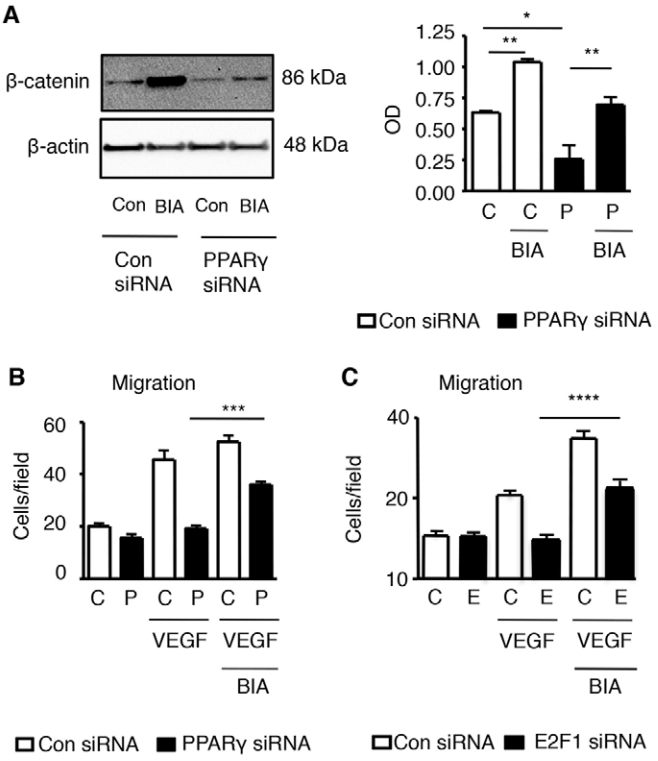

Fig. 6. Inhibition of GSKβ is able to restore β-catenin levels and rescue migration defect. (A) β-catenin protein levels of control (Non-target siRNA; 'C') and PPARγ-silenced (PPARγ siRNA; 'P') human PMVECs. PMVECs were treated with vehicle (DMSO; Con) and BIO-Acetoxime; 6-Bromoindirubin-3′-acetoxime, (BIA; 20 nM) for 6 h. Densitometry analysis was used to quantify the amount of protein per sample. (B,C) Migration assay with human PMVECs treated with PPARγ ('P'; B), E2F1 ('E'; C) and Non-target ('C'; B,C) siRNAs. Cells were stimulated with vehicle (Con), VEGF (50 ng/ml) and VEGF in combination with BIA for 6 h. Bars represent mean±s.e.m. from three separate experiments. **P*<0.05, ***P*<0.01, ****P*<0.001, *****P*<0.0001 versus respective control; one-way ANOVA with Bonferroni's multiple comparison tests in A-C.

In addition to the vascular phenotypes, adult *Tie2CrePPARγ*$^{flox/flox}$ mice show an osteopetrosis phenotype caused by dysfunctional osteoclast differentiation with increased bone mass and extramedullary hematopoiesis with splenomegaly (Wan et al., 2007). The levels of various circulating hematopoietic cells are similar in WT and *Tie2CrePPARγ*$^{flox/flox}$ mice, suggesting that extramedullary hematopoiesis is effectively compensating for decreased bone marrow production (Wan et al., 2007). This does not seem to be the case with CD34^{+}/VEGFR2^{+} cells (Fig. 1C–E). To our knowledge, this is the first report suggesting that extramedullary hematopoiesis might not compensate for EPC-like cell production, as it does for other lineages. Decreased osteoclast function could explain the accumulation of CD34^{+}/VEGFR2^{+} cells in the bone marrow, as functional osteoclasts are crucial for EPC-like cell mobilization (Aicher et al., 2008; Kollet et al., 2006). The *Tie2CrePPARγ*$^{flox/flox}$ mice represent the first animal model combining osteopetrosis and pulmonary vascular disease. Interestingly, this connection has been described in malignant infantile osteopetrosis syndrome (Kasow et al., 2004).

Whereas impaired osteoclast differentiation in *Tie2CrePPARγ*$^{flox/flox}$ mice can be rescued by bone marrow transplantation (Wan et al., 2007) and despite the phenotypic switch in CD34^{+}/VEGFR2^{+} levels in WT and *Tie2CrePPARγ*$^{flox/flox}$ mice (Fig. 1F–H), we could not rescue the impaired angiogenesis (Fig. 1I). These observations suggest that the angiogenic defect is caused by dysfunctional mature endothelium. The migratory capacity of mature endothelial cells correlates with the magnitude of neovascularization of matrigel plugs (Rohan et al., 2000). Our results are in concert with this study as PVMECs isolated from the *Tie2CrePPARγ*$^{flox/flox}$ mice also showed reduced migratory capacity and tube formation in culture (Fig. 2A–C).

Apelin, an important factor in angiogenesis, is a novel downstream target of BMP2-mediated activation of PPARγ in endothelial cells (Alastalo et al., 2011). Decreased *apelin* expression in pulmonary endothelial cells impairs migration, proliferation and survival. Furthermore, PMVECs isolated from *Tie2CrePPARγ*$^{flox/flox}$ mice show lower levels of apelin when compared with control mice (Alastalo et al., 2011). Apelin can partially rescue BMP2-stimulated PMVEC function despite reduced levels of the upstream molecule PPARγ (Fig. 3A). Our results are in line with a previous report in which stimulation with apelin combined with VEGF is shown to restore angiogenic capacity in the retina of *apelin*-deficient mice (Kasai et al., 2008). The observation that apelin did not fully rescue the angiogenic response to the level seen with BMP2 alone in WT animals (Fig. 3A), suggests that other PPARγ-associated mechanisms are required for full angiogenic capacity of PMVECs both in mice and humans (Fig. 3A,B). In several studies, increasing BMPR2 signaling and apelin expression has been shown to be beneficial in PAH (Alastalo et al., 2011; Bertero et al., 2014; Nickel et al., 2015; Spiekerkoetter et al., 2013). Our results are in line with these previous findings. However, a recent report indicates that BMP9 actually inhibits *apelin* expression (Larrivée et al., 2012; Poirier et al., 2012; Ricard et al., 2012). As these ligands use different receptors and recruit different co-receptors (Miyazono et al., 2010), downstream signaling pathways and gene regulation might differ. Future comparative studies are necessary to extend these differences, considering that BMP9 has been proposed as a therapy for PAH (Long et al., 2015).

Our RNA sequencing analysis of *PPARγ*-depleted PMVECs identified a significant enrichment of genes associated with cell-cycle control (Tables S2, S3). The Wnt–β-catenin pathway acts in concert with other signaling cascades, such as the BMP and VEGF signaling pathways, serving to affect vascular development, endothelial specification, and vascular homeostasis. Activation of the Wnt–β-catenin pathway is followed by a series of events, in which a protein complex formed by GSK3β, Axin, and adenomatous polyposis coli (APC) plays a crucial role in regulating levels of β-catenin (Adams and Alitalo, 2007). The gene expression profile after *PPARγ*-depletion in human PMVECs reflects suppression of this pathway, as we saw significant upregulation of antagonists of the Wnt pathway, such as *neucrin*, *LRP1*, *TCF7L1* and *APC2*, and suppression of Wnt activators, such as *OSTM1*, *SMAD3*, *GSKIP*, *CCND2* and *PPP2R5C* (Table S1A,B; Table S4). Whereas *neucrin* and *LRP1* directly inhibit β-catenin–Wnt signaling (Miyake et al., 2009; Su et al., 2009; Zilberberg et al., 2004), *TCF7L1* transcriptionally represses targets of canonical Wnt signaling (Cristancho et al., 2011), and APC2 inhibits Wnt signaling through proteasomal degradation (Kunttas-Tatli et al., 2012). Our RNA sequencing analysis revealed a downregulation of *SMAD3* expression. Under normal conditions, SMAD3 facilitates β-catenin nuclear translocation (Zhang et al., 2010). Furthermore, RNA sequencing analysis suggests a significant attenuation of *CCND1* expression in *PPARγ*-silenced PMVECs (Table S1B). *CCND2* is commonly upregulated upon Wnt activation associated with proliferation, (Yasui et al., 2006), whereas downregulation of *PPP2R5C* inhibits cell proliferation (Chen et al., 2013). Moreover,

Journal of Cell Science (2016) 129, 693-705 doi:10.1242/jcs.169011

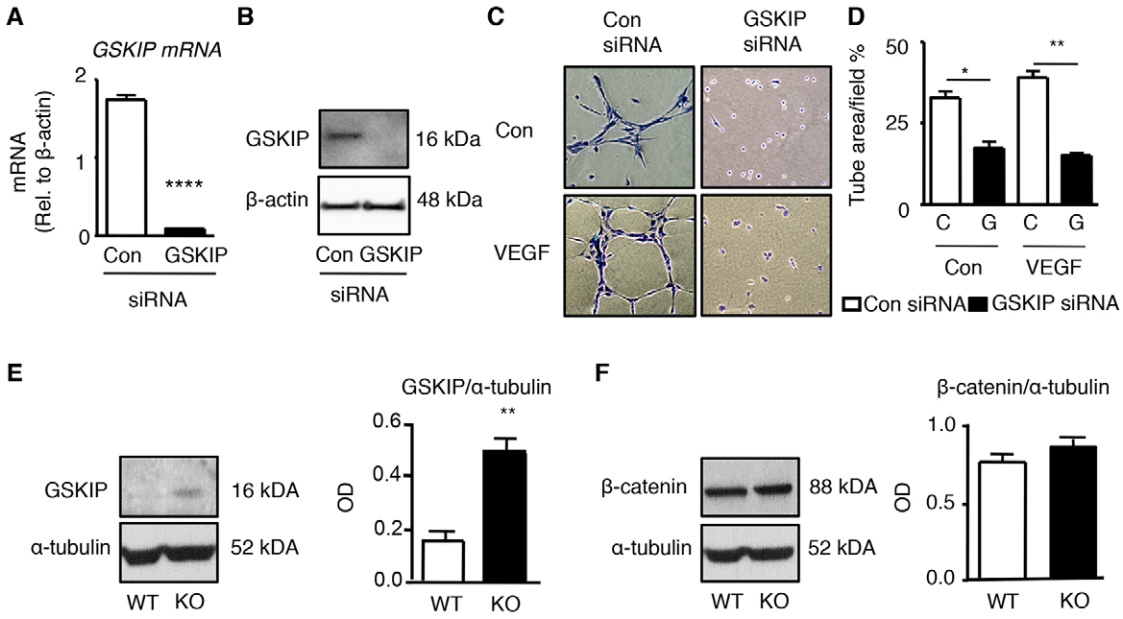

Fig. 7. Loss of GSKIP leads to severe angiogenic defect *in vitro*. (A,B) Analysis of GSKIP (A) mRNA and (B) protein expression levels 48 h after initiation of siRNA transfections. (C) *In vitro* angiogenesis assay of human PMVECs transfected with Non-target (Con) and GSKIP siRNA. Cells were stimulated with vehicle (H_2O; Con) and VEGF (50 ng/ml) for 16 h. (D) Tube formation was quantified by tube area per total field area (10× magnification) from three different fields per experiment. (E,F) Protein expression levels of (E) GSKIP and (F) β-catenin in PMVECs isolated from wild-type (WT) and *Tie2CrePPARγ*$^{flox/flox}$ (KO) mice. Densitometry analysis was used to quantify the amount of protein per sample. Error bars represent mean±s.e.m. from three separate experiments. **P*<0.05, ***P*<0.01, *****P*<0.0001 versus respective control; unpaired two-tailed *t*-test in A,E,F; one-way ANOVA with Bonferroni's multiple comparison tests in D.

reduced OSTM1 levels are commonly found in osteopetrosis patients as well as in PPARγ-deficient mice, and mutations in OSTM1 are associated with hereditary osteopetrosis. Although beyond the scope of this study, it would be interesting to evaluate the role of alterations in the Wnt pathway on the osteopetrosis disease developed by *PPARγ*-deficient mice.

GSKIP, an interesting Wnt signaling molecule, is known to directly bind to GSK3β and inactivate it by phosphorylation at position Ser9. In neuronal cells, GSKIP promotes cell-cycle progression by increasing the accumulation of β-catenin through inactivation of GSK3β (Chou et al., 2006; Lin et al., 2009), thereby promoting Wnt–β-catenin signaling in the regulation of vascular growth by promoting cell migration and survival (Hundsrucker et al., 2010; Kim et al., 2002). In the *PPARγ*-depleted human PMVECs, suppression of GSKIP is associated with constitutively active GSK3β and decreased levels of β-catenin (Fig. 5A–D).

Depletion of PPARγ in PMVECs did not affect *CTNNB1* (encoding β-catenin) gene expression (Table S1A,B), but did result in enhanced β-catenin degradation. Basal degradation of β-catenin occurs constitutively in the absence of pathway activation. When GSK3β is inhibited, β-catenin accumulates and translocates to nucleus to activate the transcription of target genes (Dejana, 2010). Despite attenuated PPARγ–E2F1, in the *Tie2CrePPARγ*$^{flox/flox}$ mice, we observed elevated GSKIP levels in PMVECs (Fig. 7E). We hypothesize that this represents activation of a compensatory mechanism associated with loss of PPARγ and E2F1 expression (Fig. 4C). Future studies are required to understand whether elevated GSKIP accounts for the milder phenotype in the *Tie2CrePPARγ*$^{flox/flox}$ PMVECs compared with the *PPARγ*-deficient human PMVECs, and whether this is the main signaling pathway also in mice.

β-catenin is an important regulator of survival and proliferation in endothelial cells (de Jesus Perez et al., 2009) and interacts with PPARγ (Alastalo et al., 2011). In contrast to our suggestion that the complex formed between PPARγ and β-catenin is transcriptionally active, Liu et al. reported that PPARγ binds β-catenin to mediate the degradation of β-catenin (Liu et al., 2006). However, in our study, PPARγ-depletion did not increase the stability of β-catenin, but rather led to decreased β-catenin protein levels (Fig. 5C,D). Based on the present and a previous study, PPARγ directly associates with β-catenin to regulate transcription, and can also modulate the downstream pathways that sustain critical levels of β-catenin. Our hypotheses were supported by experiments with the inhibitors of GSK3β that restored β-catenin levels and partially rescued the migratory defect in *PPARγ*-deficient human PMVECs (Fig. 6A,B; Fig. S4A,B).

Various bioinformatics approaches together with ChIP analysis suggested *E2F1* as a direct target of PPARγ and a potential regulator of *GSKIP*. There is increasing evidence that E2Fs function as transcriptional regulators of angiogenesis-associated genes. Suppression of E2F1 reduces VEGF-stimulated angiogenic tube formation (Pillai et al., 2010), a result correlating well with our observations. Our results suggest a regulatory feedback loop between E2F1 and PPARγ, as PPARγ is able to occupy the *E2F1* promoter area (Fig. S2A,B) and suppression of PPARγ leads to attenuated expression of *E2F1* (Fig. 4A–C). The *E2F1* promoter area showing PPARγ occupancy in ChIP-chip (Alastalo et al., 2011) and in ChIP analysis (Fig. S2B) did not show classical PPRE binding motifs. This is not surprising as 40% of identified PPARγ binding sites in genome-wide ChIP analyses do not harbor classical PPREs, suggesting that PPARγ can bind other motifs or interact with DNA through co-factors (Alastalo et al., 2011). Interestingly, the previous ChIP-chip analysis revealed the co-occupancy of β-catenin in the same region of the *E2F1* promoter (Alastalo et al., 2011). Previous studies have established a link between E2F1 and PPARγ in adipogenesis, in which E2F1 and PPARγ are co-expressed during adipose cell differentiation, and in brain cancer cells, in which E2F1 is able to induce PPARγ expression (Bhatia et al., 2012; Fajas et al., 2002). In PMVECs, a similar regulation loop between E2F1 and PPARγ was not observed.

Journal of Cell Science (2016) 129, 693-705 doi:10.1242/jcs.169011

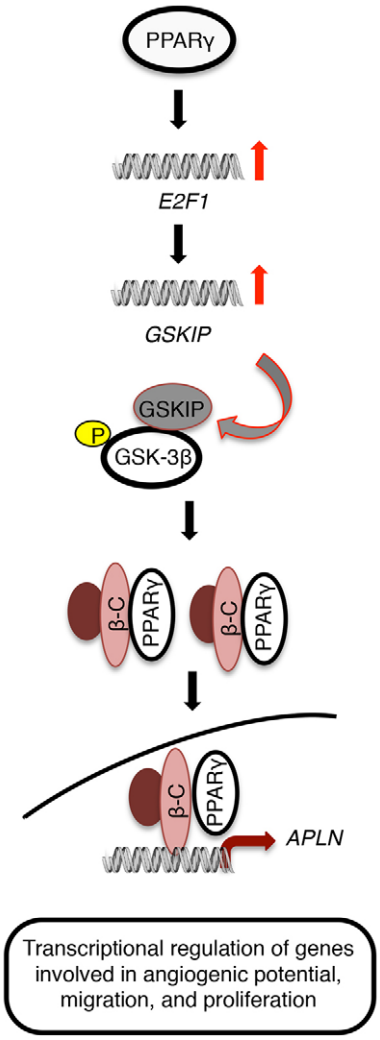

Fig. 8. Hypothetical model explaining the dysfunctional Wnt–β-catenin signaling in PPARγ deficiency. We propose a model where loss of PPARγ leads to impaired angiogenesis through a dysfunctional Wnt–β-catenin signaling pathway. PPARγ contributes to the activity of the Wnt–β-catenin signaling pathway by regulating *E2F1* expression, which is essential in sustaining critical levels of GSKIP in PMVECs and contributes to the migration capacity of PMVECs. GSKIP inhibits GSK3β to inactivate the degradation complex of β-catenin (β-C). This allows β-catenin to accumulate and form complexes with its co-factors such as PPARγ (Alastalo et al., 2011). The PPARγ–β-catenin complex translocates into the nucleus and regulates genes important for endothelial cell homeostasis. APLN, apelin.

In conclusion, we propose a model in which loss of PPARγ leads to impaired angiogenesis through downregulation of E2F1 and dysfunctional Wnt–β-catenin signaling and gene regulation (Fig. 8). In this model the cross-talk between the Wnt pathway and PPARγ is not only mediated through physical complex formation between PPARγ and β-catenin (Alastalo et al., 2011) but PPARγ can sustain a cellular milieu optimal for normal endothelial cell function through regulation of Wnt pathway components, such as GSKIP. Future studies are needed to assess the biological significance of these observations in other cell types and disease conditions and to fully understand the regulation of Wnt pathway components in *PPARγ*-deficient endothelial cells. We also need more studies to reveal whether E2F1 is a direct regulator of GSKIP, as the promoter of *GSKIP* harbors an E2F1 binding motif (Table S5).

MATERIALS AND METHODS

All of the animal procedures were performed in compliance with the appropriate National Animal Experiment Board in Finland and by the Animal Care Committee of Stanford University, in keeping with the regulations of the American Physiological Society.

In vivo angiogenesis assay

The creation and phenotypic characterization of *Tie2CrePPARγ*$^{flox/flox}$ mice has been previously described (Kisanuki et al., 2001; He et al., 2003; Guignabert et al., 2009) (Tie2-Cre is also called Tek-Cre). Littermates were used as controls. A 500 µl aliquot of liquefied matrigel (Becton Dickinson Oy, Vantaa, Finland) containing vehicle (H_2O) and BMP2 (10 ng/ml) were injected subcutaneously into anesthetized (avertin+ketamin) 12–15-week-old wild-type (WT) and *Tie2CrePPARγ*$^{flox/flox}$ mice. Three plugs per mouse were injected subcutaneously into the back of the mice and then removed after 21 days. All three plugs per mouse contained the same experimental conditions. The plugs were fixed in 10% formalin for 12 h and stained with Hematoxylin and Eosin (H&E) to identify blood-filled endothelial cell channels. The number of vessels with red cells per field was quantified under a microscope (20× magnification) (Kano et al., 2005). The technology has been previously described and validated by de Jesus Perez et al. (2009). As a control, immunofluorescence was used to show microvessel formation at 40× magnification in matrigel plugs implanted into WT mice by labeling murine CD31 with a GFP-conjugated antibody and staining nuclei with DAPI (Fig. S1A).

Flow cytometric analysis of CD34$^+$/VEGFR2$^+$ cells

Murine CD34$^+$/VEGFR2$^+$ cells were determined by flow activated cell sorting (FACS; Calibur Instrument, BD Biosciences, San Jose, CA) using a panel of fluorochrome-conjugated monoclonal antibodies reacting with CD45 (1 µg/ml; #559864, APC) or endothelial markers VEGFR2 (1 µg/ml; #555308) and CD34 (1 µg/ml; #560238) (Schuch et al., 2003; Asahara et al., 1999; Chakroborty et al., 2008). Blood from WT and *Tie2CrePPARγ*$^{flox/flox}$ mice was collected for analysis of circulating CD34$^+$/VEGFR2$^+$ cells. Spleen cells were isolated by mechanical disruption by passing the tissue through a cell strainer using a plunger. Bone marrow cells were isolated as described below. Following red cell lysis, CD34$^+$/VEGFR2$^+$ cells were enumerated by flow cytometry using gates to exclude dead cells, debris and platelets. The percentage of stained cells was finally determined after comparison with matched isotype controls. Corresponding isotype controls were performed using the following antibodies: APC rat IgG2b (1 µg/ml; # 556924), PE Rat IgG2a (1 µg/ml; #553930), FITC Rat IgG2a (1 µg/ml; #553929). CD16/CD32 was used to block non-specific binding (1 µg/ml; #552140). All specific and isotype control antibodies were from BD Biosciences.

Bone marrow transplantation

Donor mice (8–12 weeks old) were euthanized and both left and right femur and tibia were removed and cleaned of all soft tissue. The ends of each bone were removed and the bone marrow was collected, filtered, washed, and viable cells were counted. Six-week-old recipient mice were irradiated with lethal 950 cGy, delivered in two fractions. After the last irradiation, mice received donor bone marrow cells through tail vein injection and were analyzed 12 weeks after transplantation. WT mice were transplanted with *PPARγ*-deficient bone marrow isolated from *Tie2CrePPARγ*$^{flox/flox}$ mice and *Tie2CrePPARγ*$^{flox/flox}$ mice were transplanted with WT bone marrow. Three weeks before analysis matrigel plugs were injected to study angiogenic capacity of these mice.

Isolation of mouse pulmonary microvascular endothelial cells

PMVECs were isolated by digesting whole lung tissue with collagenase IA (0.5 mg/ml, Sigma-Aldrich, Helsinki, Finland) for 45 min at 37°C. The cell suspension was filtered through cell strainers and centrifuged at 250 ***g*** for 5 min. The cell pellet was washed with 1×PBS and the cell suspension was incubated with sheep anti-rat IgG magnetic beads (Invitrogen, Life Technologies, Helsinki, Finland) coated with rat anti-mouse CD31 antibody to select out PMVECs for culture. Characterization of the cell culture after endothelial cell isolation was performed by labeling with Dil-conjugated Ac-LDL (Dil–Ac-LDL) and CD31 staining. This staining

Journal of Cell Science (2016) 129, 693-705 doi:10.1242/jcs.169011

showed over 95% purity for endothelial cells (Alastalo et al., 2011; Guignabert et al., 2009).

Cell culture

PMVECs (human EC-L, Sciencell Research Laboratories, Carlsbad, CA) were grown on commercial EGM-2 media (Lonza Clonetics, Fisher Scientific Oy, Vantaa, Finland) in gelatin-coated dishes. All PMVECs used in experiments were authenticated and tested for contamination.

In vitro angiogenesis assay

In vitro tube formation was assessed using The Cultrex *In vitro* Angiogenesis Assay Kit following manufacturer's protocol (Trevigen, Gaithersburg, MD). Cells were first counted, then PMVECs in starvation media containing either vehicle (H_2O), BMP2 (10 ng/ml), or VEGF (50 ng/ml) were plated into 24-well plates coated with Reduced Growth Factor Basement Membrane Extract (Trevigen). For all experiments performed with WT and *Tie2CrePPARγ*$^{flox/flox}$ mice, representative images of endothelial tube networks were obtained at 16 h under a fluorescence microscope, and the total tube area per field at 10× magnification was quantified in a blinded fashion using Bioquant Image Analysis software (R&M Biometrics, Nashville, TN). Calcein pre-treatment was used to fluorescently label all living murine PMVECs (Trevigen). In experiments performed with human PMVECs, cells were first fixed and stained following the protocol provided by the manufacturer (Trevigen) and the identification of endothelial tube formation was done under a light microscope (10× magnification) from three different fields. The total tube area per field at 10× magnification was quantified using Wimasis Image Analysis software (Wimasis GmbH, Munich, Germany).

In vitro migration assay

To assess cell migration, we used the modified Boyden chamber assay. Either mouse or human PMVECs were added to gelatin-coated microporous inserts in 24-well plates and the migratory stimulus [vehicle was H_2O, except when BIA was used - then vehicle was DMSO; BMP2 (10 ng/ml), VEGF (50 ng/ml), apelin (100 nM; American Peptide Company, Derbyshire, UK), BIO-Acetoxime; 6-Bromoindirubin-3′-acetoxime, (BIA; 20 nM; Santa Cruz Biotechnology, Heidelberg, Germany), or LiCl (10 mM; Sigma-Aldrich)] was added to the well in the bottom of the chamber and incubated at 37°C for 6 h. The cells that had migrated through the bottom of the insert were fixed and stained with the Diff Quick Kit (Fischer Scientific) and were counted under a microscope (20× magnification). Three different fields at the center of each well were counted.

RNAi

The first 750 µl of Opti-Mem was mixed with 9.3 µl of RNAiMAX Lipofectamine and incubated for 5 min. The second 750 µl of Opti-MEM was mixed with specific siRNAs to final concentration of 100 nM. The two mixtures were then pooled and incubated for 20 min. Cells were divided 24 h before siRNA-transfections. Lipofectamine RNAiMax reagent (Invitrogen/Thermo Scientific) was mixed in 750 µl of Opti-MEM (Gibco/Thermo Scientific) and incubated for 5 min at room temperature. On-target plus Non-targeting siRNAs (D-001810-01-20), On-target plus Smart pool, human PPARγ siRNAs (L-003436-00-0010), On-target plus Smart pool, human E2F1 (L-003259-00-0010), and human On-target plus GSKIP (L-020252-02-0010) siRNAs purchased from Dharmacon (Thermo Scientific) were added to 750 µl of Opti-MEM to a final concentration of 100 nM before mixing with Lipofectamine RNAiMax reagent and the mixture incubated 20 min at room temperature. The transfection mixture was then added to cells and incubated at 37°C for 6 h. After incubation, 5 ml of EGM-2 media was added to the endothelial cells, and the cells incubated further until harvest at 48 h after the beginning of transfection. Knockdown of PPARγ, E2F1 and GSKIP was determined by quantitative real-time PCR (qRT-PCR) and by western immunoblotting (Fig. S1B,C, Fig. S2C,D; Fig. 7A,B).

Gene expression analysis

RNA was isolated using the Nucleospin RNA II Kit (Macherey-Nagel, BiotTop oy, Turku, Finland) and reverse transcribed by Reverse Transcription Core Kit (Eurogentec, Seraing, Belgium) following manufacturer's instructions. qPCR was performed using MESA Green qPCR Mastermix Plus for SYBR® Assay (Eurogentec) with a 7900HT Fast Real-Time PCR System detector (Applied Biosystems, Espoo, Finland). Expression levels were quantified using primer sets from Oligomer (Helsinki, Finland) and Integrated DNA Technologies (Leuven, Belgium). β-actin mRNA expression was used for the normalization of the mRNA expression levels of specific genes. Primers used in qPCR experiments are summarized in Table S6.

Proliferation and survival assays

PMVECs were transfected with Non-target and PPARγ siRNAs as previously described. 24 h after initiation of transfections PMVECs were seeded into 24- and 96-well plates and allowed to adhere. To demonstrate equal loading of PMVECs into each well, cells under control conditions were allowed to adhere for 6 h before the amount of cells was validated. For proliferation experiments PMVECs transfected with Non-target and PPARγ siRNA were starved under serum-free conditions for 6 h before adding 4% serum into each well. Cells were left to recover overnight. In cell count experiments, cells were detached and counted under a microscope. An MTT proliferation assay was performed following the manufacturer's instructions (Promega Biotech, Nacka, Sweden). For survival experiments PMVECs transfected with both Non-target and PPARγ siRNA were starved under serum-free conditions for 6 h. Caspase-Glo® 3/7 Assay were done following the protocol provided by Promega.

Western immunoblotting

Protein lysates were prepared by adding boiling lysis buffer (10 mM Tris-HCl, 1% SDS, 0.2 mM PMSF) including protease and phosphatase inhibitors (Sigma-Aldrich), and lysates were boiled for 10 min, centrifuged, and the supernatants collected. Equal amounts of protein were loaded onto the wells of Bolt® 4–12% Bis-Tris gels (Novex, Life Technologies, Helsinki, Finland), and subjected to electrophoresis under reducing conditions. Gels were blotted to nitrocellulose membranes (Millipore, Billerica, MA), which were blocked with either 5% milk–TBS containing 0.1% Tween or 5% BSA–TBS with 0.1% Tween. Primary antibodies: rabbit anti-PPARγ (1:300; Cell Signaling Technology Europe, Leiden, The Netherlands; #2435), rabbit anti-phosphoGSK3β (Ser9) (1:500; Cell Signaling, #9336), rabbit anti-GSK3β (1:1000; Cell Signaling, #9315). Cell Signaling, #9336), rabbit anti-GSK3β (1:1000; Cell Signaling, #9315), rabbit anti-GSKIP (1:1000; Novus Biologicals, Hämeenlinna, Finland; #NBP1-79653), rabbit anti-β-catenin (1:800; Millipore, #ABE208), rabbit anti-E2F1 (1:500; Cell Signaling, #3742 and 1:500; Abcam, #ab137415), rabbit anti-phosphoVEGFR2 (1:300; Cell Signaling, #2478), mouse anti-Flk-1 (1:500; Santa Cruz Biotechnologies, SC-6251), and goat anti-actin (1:1000; Santa Cruz Biotechnologies, SC-1615) were incubated overnight at 4°C. Membranes were washed with 1×TBS containing 0.1% Tween before incubation with secondary horseradish peroxidase (HRP)-conjugated antibodies (1:10,000; Santa Cruz Biotechnologies; #SC-2030, SC-2031, SC-2033). Visualization was performed using ECL (PerkinElmer, Waltham, MA) or ECL prime (GE Healthcare Finland, Helsinki, Finland). Densitometry was performed to quantify protein amount per sample using ImageJ software (NIH, Bethesda, MD). Normalization was performed against β-actin or α-tubulin protein expression.

RNA-sequence sample preparation

For RNA sequencing cells were transfected with either Non-target siRNAs or PPARγ siRNAs and harvested 48 h after transfections, as described previously. Samples were purified using NucleoSpin® RNA Clean-up kit (Macherey-Nagel). RNA samples were prepared for Illumina RNA sequencing using instructions provided by New England BioLabs (NEB; Ipswich, MA) with the help of the Biomedicum Functional Genomics Unit (FuGU, Helsinki, Finland). Total of 1–5 µg RNA was used as starting material. Isolation of poly(A)+ RNA transcripts from total RNA for RNA library preparation and sequencing was done using NEBNext Oligo $d(T)_{25}$ magnetic beads (NEB). After RNA isolation, samples were fragmented followed by clean up with RNeasy MinElute Clean-up Kit (Qiagen Nordic,

Helsinki, Finland) following manufacturer's instructions. RNA fragments were synthesized to double-stranded cDNA followed by the purification of the samples with 1.8× Agencourt AMPure XP Beads (Beckman Coulter, Vantaa, Finland). RNA sequencing was done in collaboration with Institute of Molecular Medicine Finland (FIMM, Helsinki, Finland) using The Illumina HighSeq® 2000 System (Illumina, San Diego, CA) with pair-end cluster (100 bp) in one lane.

RNA sequence data processing

Read alignment and abundance calculation

The quality of the raw fastq sequence from the sequencer was checked by subjecting raw paired-end sequence reads to pre-processing and post-processing quality checks using FastQC tool (http://www.bioinformatics.babraham.ac.uk/projects/fastqc/). Reads quality trimming and adapter sequence removal were carried out using Trimmomatic in paired-end mode (Bolger et al., 2014). High-quality reads were mapped to human genome reference sequence build hg19 using fast and accurate read alignment with Burrows–Wheeler transformation (BWA) (Li and Durbin, 2009). The abundance of mRNAs for all annotated genes from the ENSEMBL v72 annotation of the human genome (hg19) was calculated using an in-house R script. The R script was used to count the number of reads that mapped to each annotated gene, allowing, in some cases, for reads to partially overlap with the exons and still be counted for that gene (i.e. union). The counts for all the samples were collated into one file and any gene with fewer than five reads in all samples was excluded from the subsequent statistical analysis of differential gene expression.

Identification of SDEG genes and pathway analysis

Significantly differentially expressed genes were identified using edgeR, DESeq and baySeq packages (Bioconductor) and applying built-in procedures for library normalization and estimation of variance (Anders and Huber, 2010; Hardcastle 2010; Robinson et al., 2010). The statistical tests in each analysis were corrected for multiple testing using the Benjamini and Hochberg (BH) method (Benjamini and Hochberg, 1995) as implemented in R (version 3.0.0). Genes detected by at least two out of three methods with $P<0.05$ and FDR<0.01 were regarded as being significantly differentially expressed (SDE). All genes that were found to be significantly differentially expressed between the two experimental conditions were retained for further analysis. GOstats and KEGG pathway analysis tools were used to identify biological pathways that were significantly enriched in the dataset of SDE genes (Falcon and Gentleman, 2007). Hypergeometric tests with Benjamini and Hochberg false discovery rate (FDR) were performed to adjust the *P*-value. RNA sequencing data is available in the GEO database under accession number GSE62982.

In silico transcription factor binding site analyses

Transcription factor binding site (TFBS) enrichment analysis of vertebrate transcription factors was performed using the oPOSSUM single site analysis tool (Ho Sui et al., 2007). The following threshold criteria were used: a *z*-score at least 10 and a Fisher score at most 0.01. TFBS near the transcription start site were identified through a two-step process using data available on the UCSC genome browser (http://genome.ucsc.edu/). First, putative promoter regions were identified as intervals within 1.5 kb of the transcription start site as identified by the RefSeq Genes track, within a CpG island as identified by the CpG Island track, which had a mammalian conservation score greater than 0.5 in the Placental Mammal Conservation by PhastCons track, and overlapped at least one DNaseI footprint in one of the endothelial cell lines (umbilical vein endothelial cells; adult blood microvascular endothelial cells, dermal-derived; neonatal blood; microvascular endothelial cells, dermal-derived; neonatal lymphatic microvascular endothelial cells, dermal-derived; blood microvascular endothelial cells, lung-derived; lymphatic microvascular endothelial cells, lung-derived) in the DNaseI Digital Genomic Footprinting from ENCODE/University of Washington track. Second, these putative promoter regions were analyzed for TFBS using the Jaspar motif analysis tool (http://jaspar.genereg.net).

Chromatin immunoprecipitation assay

Chromatin immunoprecipitation (ChIP) assay was done following the instructions provided by the manufacturer using Chromatin Immunoprecipitation (ChIP) Assay Kit (Millipore). Cross-linking was done adding formaldehyde to a final concentration of 1%. After incubation for 10 min at 37°C, cells were washed with 1×PBS containing protease inhibitors. Endothelial cells were pelleted by centrifugation at 11,000 ***g*** and SDS Lysis Buffer (Millipore) was added at room temperature. Fragmentation of the DNA in lysates was done using a Covaris ultrasonicator with the sonication program provided by the manufacturer for 500 bp DNA shearing. Samples were centrifuged at 11,000 ***g***, supernatant was collected and diluted in ChIP Dilution Buffer (Millipore) including protease inhibitors. Approximately 10% of the diluted samples were stored as input samples. Nonspecific background was reduced by pre-clearing the diluted cell supernatant with Protein A Agarose/Salmon Sperm DNA (Millipore). Agarose was pelleted by brief centrifugation at 5000 ***g*** and supernatant was collected. For immunoprecipitation of PPARγ, anti-PPARγ antibody (1.5 µg/1ml of cell lysate; clone E-8; Santa Cruz Biotechnologies, #SC-7273X) was added to supernatant fractions and incubated overnight. For a negative control, no-antibody immunoprecipitation was performed by incubating the supernatant fraction with Protein A Agarose/Salmon Sperm DNA. After brief centrifugation at 5000 ***g***, supernatant was removed and the pelleted complex was washed once for 5 min with Low Salt Immune Complex Wash Buffer (Millipore), once with High Salt Immune Complex Salt Wash Buffer (Millipore), once with LiCl Immune Complex Wash Buffer (Millipore) and twice with TE Buffer (Millipore). Elution was done twice in 1% SDS and 0.1 M $NaHCO_3$. Cross-linking was reversed by adding 5 M NaCl to the eluates and heating at 65°C for 4 h. DNA samples were further purified by adding 0.5 M EDTA, 1 M Tris-HCl, and 20 mg/ml Proteinase K and incubated for an hour at 45°C. DNA was recovered by phenol/chloroform extraction and ethanol precipitation. Primers used in ChIP assay are summarized in Table S6.

Statistical analysis

Values from multiple experiments are shown as mean±s.e.m. Statistical significance was determined using either two-tailed *t*-test or one-way ANOVA followed by Bonferroni's multiple comparison test. $P<0.05$ was considered as significant. The number of samples or animals in each group is indicated in the figure legends.

Acknowledgements

We thank Lingli Wang for developing and maintaining the mouse lines.

Competing interests

The authors declare no competing or financial interests.

Author contributions

Study conception: S.V.-C., O.A., M.L., J.W.K., M.R. and T.-P.A.; hypotheses delineation and design of the study: S.V.-C., O.A., M.R. and T.-P.A.; performing experiments: S.V.-C., M.K., C.G.L., C.A., H.S., S.P.R., K.Y. and T.-P.A.; data analysis: S.V.-C., O.A., M.L.; data interpretation: S.V.-C., O.A., M.L., M.R. and T.-P.A.; drafting the manuscript: S.V.-C., O.A., M.R. and T.-P.A.; revising the manuscript: S.V.-C., O.A., M.L., M.K., C.A., C.G.L., H.S., S.P.R., K.Y., V.d.J.P., J.W.K., M.R. and T.-P.A. All authors have contributed to the manuscript and critically evaluated all versions of the manuscript. M.R. and T.-P.A. have equal senior authorship.

Funding

This work was supported by Sigrid Juselius Foundation, Finnish Medical Foundation, Finnish Foundation for Cardiovascular Research, The Finnish Research Foundation of the Pulmonary Diseases (to S.V.-C.), The Finnish Research Foundation of Aarne and Aili Turunen (to S.V.-C.), Finnish Cultural Foundation [grant 00150083 to O.A.], Biomedicum Helsinki Foundation (to S.V.-C.), Finnish Foundation for Pediatric Research, and National Institutes of Health [grant number R01-HL087118 and R01-HL074186], and the Dwight and Vera Dunlevie Endowed Professorship (to M.R.).

Supplementary information

Supplementary information available online at
http://jcs.biologists.org/lookup/suppl/doi:10.1242/jcs.169011/-/DC1

References

Adair, T. H. and Montani, J. P. (2010). *Angiogenesis*. San Rafael, USA: Morgan & Claypool Life Sciences.

Adams, R. H. and Alitalo, K. (2007). Molecular regulation of angiogenesis and lymphangiogenesis. *Nat. Rev. Mol. Cell Biol.* **8**, 464-478.
Aicher, A., Kollet, O., Heeschen, C., Liebner, S., Urbich, C., Ihling, C., Orlandi, A., Lapidot, T., Zeiher, A. M. and Dimmeler, S. (2008). The Wnt antagonist Dickkopf-1 mobilizes vasculogenic progenitor cells via activation of the bone marrow endosteal stem cell niche. *Circ. Res.* **103**, 796-803.
Alastalo, T.-P., Li, M., de Jesus Perez, J., Pham, D., Sawada, H., Wang, J. K., Koskenvuo, M., Wang, L., Freeman, B. A., Chang, H. Y. et al. (2011). Disruption of PPARgamma/beta-catenin–mediated regulation of apelin impairs BMP-induced mouse and human pulmonary arterial EC survival. *J. Clin. Invest.* **121**, 3735-3746.
Anders, S. and Huber, W. (2010). Differential expression analysis for sequence count data. *Genome Biol.* **11**, R106.
Asahara, T., Masuda, H., Takahashi, T., Kalka, C., Pastore, C., Silver, M., Kearne, M., Magner, M. and Isner, J. M. (1999). Bone marrow origin of endothelial progenitor cells responsible for postnatal vasculogenesis in physiological and pathological neovascularization. *Circ. Res.* **85**, 221-228.
Barak, Y., Nelson, M. C., Ong, E. S., Jones, Y. Z., Ruiz-Lozano, P., Chien, K. R., Koder, A. and Evans, R. M. (1999). PPAR gamma is required for placental, cardiac, and adipose tissue development. *Mol. Cell* **4**, 585-595.
Benjamini, Y. and Hochberg, Y. (1995). Controlling the false discovery rate - a practical and powerful approach to multiple testing. *J R Stat Soc Series B Stat Methodol.* **57**, 289-300.
Bertero, T., Lu, Y., Annis, S., Hale, A., Bhat, B., Saggar, R., Saggar, R., Wallace, W. D., Ross, D. J., Vargas, S. O. et al. (2014). Systems-level regulation of microRNA networks by miR-130/301 promotes pulmonary hypertension. *J. Clin. Invest.* **124**, 3514-3528.
Bhatia, B., Potts, C. R., Guldal, C., Choi, S., Korshunov, A., Pfister, S., Kenney, A. M. and Nahlé, Z. A. (2012). Hedgehog-mediated regulation of PPARgamma controls metabolic patterns in neural precursors and shh-driven medulloblastoma. *Acta Neuropathol.* **123**, 587-600.
Biscetti, F., Gaetani, E., Flex, A., Aprahamian, T., Hopkins, T., Straface, G., Pecorini, G., Stigliano, E., Smith, R. C., Angelini, F. et al. (2008). Selective activation of peroxisome proliferator-activated receptor (PPAR)alpha and PPAR gamma induces neoangiogenesis through a vascular endothelial growth factor-dependent mechanism. *Diabetes* **57**, 1394-1404.
Bishop-Bailey, D. (2011). PPARs and angiogenesis. *Biochem. Soc. Trans.* **39**, 1601-1605.
Bolger, A. M., Lohse, M. and Usadel, B. (2014). Trimmomatic: a flexible trimmer for Illumina sequence data. *Bioinformatics* **30**, 2114-2120.
Calkin, A. C. and Thomas, M. C. (2008). PPAR agonists and cardiovascular disease in diabetes. *PPAR Res.* **2008**, 245410.
Chakroborty, D., Chowdhury, U. R., Sarkar, C., Baral, R., Dasgupta, P. S. and Basu, S. (2008). Dopamine regulates endothelial progenitor cell mobilization from mouse bone marrow in tumor vascularization. *J. Clin. Invest.* **118**, 1380-1389.
Chen, Y., Liu, S., Shen, Q., Zha, X., Zheng, H., Yang, L., Chen, S., Wu, X., Li, B. and Li, Y. (2013). Differential gene expression profiles of PPP2R5C-siRNA-treated malignant T cells. *DNA Cell Biol.* **32**, 573-581.
Chou, H.-Y., Howng, S.-L., Cheng, T.-S., Hsiao, Y.-L., Lieu, A.-S., Loh, J.-K., Hwang, S.-L., Lin, C.-C., Hsu, C.-M., Wang, C. et al. (2006). GSKIP is homologous to the Axin GSK3beta interaction domain and functions as a negative regulator of GSK3beta. *Biochemistry* **45**, 11379-11389.
Ciarrocchi, A., Jankovic, V., Shaked, Y., Nolan, D. J., Mittal, V., Kerbel, R. S., Nimer, S. D. and Benezra, R. (2007). Id1 restrains p21 expression to control endothelial progenitor cell formation. *PLoS ONE* **2**, e1338.
Cristancho, A. G., Schupp, M., Lefterova, M. I., Cao, S., Cohen, D. M., Chen, C. S., Steger, D. J. and Lazar, M. A. (2011). Repressor transcription factor 7-like 1 promotes adipogenic competency in precursor cells. *Proc. Natl. Acad. Sci. USA* **108**, 16271-16276.
David, L., Feige, J.-J. and Bailly, S. (2009). Emerging role of bone morphogenetic proteins in angiogenesis. *Cytokine Growth Factor Rev.* **20**, 203-212.
de Jesus Perez, V. A., Alastalo, T.-P., Wu, J. C., Axelrod, J. D., Cooke, J. P., Amieva, M. and Rabinovitch, M. (2009). Bone morphogenetic protein 2 induces pulmonary angiogenesis via Wnt-beta-catenin and Wnt-RhoA-Rac1 pathways. *J. Cell Biol.* **184**, 83-99.
Dejana, E. (2010). The role of wnt signaling in physiological and pathological angiogenesis. *Circ. Res.* **107**, 943-952.
Delgado, V. M. C., Nugnes, L. G., Colombo, L. L., Troncoso, M. F., Fernandez, M. M., Malchiodi, E. L., Frahm, I., Croci, D. O., Compagno, D., Rabinovich, G. A. et al. (2011). Modulation of endothelial cell migration and angiogenesis: a novel function for the "tandem-repeat" lectin galectin-8. *FASEB J.* **25**, 242-254.
Desouza, C. V., Rentschler, L. and Fonseca, V. (2009). Peroxisome proliferator-activated receptors as stimulants of angiogenesis in cardiovascular disease and diabetes. *Diabetes Metab. Syndr. Obes.* **2**, 165-172.
Duan, S. Z., Ivashchenko, C. Y., Usher, M. G. and Mortensen, R. M. (2008). PPAR-gamma in the cardiovascular system. *PPAR Res.* **2008**, 745804.
Fajas, L., Landsberg, R. L., Huss-Garcia, Y., Sardet, C., Lees, J. A. and Auwerx, J. (2002). E2Fs regulate adipocyte differentiation. *Dev. Cell* **3**, 39-49.
Falcon, S. and Gentleman, R. (2007). Using GOstats to test gene lists for GO term association. *Bioinformatics* **23**, 257-258.
Feigin, M. E. and Malbon, C. C. (2008). OSTM1 regulates beta-catenin/Lef1 interaction and is required for Wnt/beta-catenin signaling. *Cell. Signal.* **20**, 949-957.
Gerhardt, H. (2008). VEGF and endothelial guidance in angiogenic sprouting. *Organogenesis* **4**, 241-246.
Goodwin, A. M. and D'Amore, P. A. (2002). Wnt signaling in the vasculature. *Angiogenesis* **5**, 1-9.
Guignabert, C., Alvira, C. M., Alastalo, T.-P., Sawada, H., Hansmann, G., Zhao, M., Wang, L., El-Bizri, N. and Rabinovitch, M. (2009). Tie2-mediated loss of peroxisome proliferator-activated receptor-gamma in mice causes PDGF receptor-beta-dependent pulmonary arterial muscularization. *Am. J. Physiol. Lung Cell. Mol. Physiol.* **297**, L1082-L1090.
Hardcastle, T. J. and Kelly, K. A. (2010). baySeq: Empirical Bayesian analysis of patterns of differential expression in count data. *BMC Bioinformatics* **11**, 422.
He, W., Barak, Y., Hevener, A., Olson, P., Liao, D., Le, J., Nelson, M., Ong, E., Olefsky, J. M. and Evans, R. M. (2003). Adipose-specific peroxisome proliferator-activated receptor gamma knockout causes insulin resistance in fat and liver but not in muscle. *Proc. Natl. Acad. Sci. USA* **100**, 15712-15717.
Ho Sui, S. J., Fulton, D. L., Arenillas, D. J., Kwon, A. T., and Wasserman, W. W. (2007). oPOSSUM: integrated tools for analysis of regulatory motif over-representation. *Nucleic Acids Res.* **35**, W245-W252.
Hundsrucker, C., Skroblin, P., Christian, F., Zenn, H.-M., Popara, V., Joshi, M., Eichhorst, J., Wiesner, B., Herberg, F. W., Reif, B. et al. (2010). Glycogen synthase kinase 3beta interaction protein functions as an A-kinase anchoring protein. *J. Biol. Chem.* **285**, 5507-5521.
Kano, M. R., Morishita, Y., Iwata, C., Iwasaka, S., Watabe, T., Ouchi, Y., Miyazono, K. and Miyazawa, K. (2005). VEGF-A and FGF-2 synergistically promote neoangiogenesis through enhancement of endogenous PDGF-B-PDGFRbeta signaling. *J. Cell Sci.* **118**, 3759-3768.
Kasai, A., Shintani, N., Kato, H., Matsuda, S., Gomi, F., Haba, R., Hashimoto, H., Kakuda, M., Tano, Y. and Baba, A. (2008). Retardation of retinal vascular development in apelin-deficient mice. *Arterioscler. Thromb. Vasc. Biol.* **28**, 1717-1722.
Kasow, K. A., Bonfim, C., Asch, J., Margolis, D. A., Jenkins, J., Tamburro, R. F., Handgretinger, R. and Horwitz, E. M. (2004). Malignant infantile osteopetrosis and primary pulmonary hypertension: a new combination? *Pediatr. Blood Cancer* **42**, 190-194.
Kim, H.-S., Skurk, C., Thomas, S. R., Bialik, A., Suhara, T., Kureishi, Y., Birnbaum, M., Keaney, J. F. J. and Walsh, K. (2002). Regulation of angiogenesis by glycogen synthase kinase-3beta. *J. Biol. Chem.* **277**, 41888-41896.
Kim, K. Y., Ahn, J. H. and Cheon, H. G. (2011). Anti-angiogenic action of PPARgamma ligand in human umbilical vein endothelial cells is mediated by PTEN upregulation and VEGFR-2 downregulation. *Mol. Cell. Biochem.* **358**, 375-385.
Kisanuki, Y. Y., Hammer, R. E., Miyazaki, J.-i., Williams, S. C., Richardson, J. A. and Yanagisawa, M. (2001). Tie2-Cre transgenic mice: a new model for endothelial cell-lineage analysis in vivo. *Dev. Biol.* **230**, 230-242.
Kollet, O., Dar, A., Shivtiel, S., Kalinkovich, A., Lapid, K., Sztainberg, Y., Tesio, M., Samstein, R. M., Goichberg, P., Spiegel, A. et al. (2006). Osteoclasts degrade endosteal components and promote mobilization of hematopoietic progenitor cells. *Nat. Med.* **12**, 657-664.
Kunttas-Tatli, E., Zhou, M.-N., Zimmerman, S., Molinar, O., Zhouzheng, F., Carter, K., Kapur, M., Cheatle, A., Decal, R. and McCartney, B. M. (2012). Destruction complex function in the Wnt signaling pathway of Drosophila requires multiple interactions between Adenomatous polyposis coli 2 and Armadillo. *Genetics* **190**, 1059-1075.
Lamalice, L., Le Boeuf, F. and Huot, J. (2007). Endothelial cell migration during angiogenesis. *Circ. Res.* **100**, 782-794.
Larrivée, B., Prahst, C., Gordon, E., del Toro, R., Mathivet, T., Duarte, A., Simons, M. and Eichmann, A. (2012). ALK1 signaling inhibits angiogenesis by cooperating with the Notch pathway. *Dev. Cell* **22**, 489-500.
Li, H. and Durbin, R. (2009). Fast and accurate short read alignment with Burrows-Wheeler transform. *Bioinformatics* **25**, 1754-1760.
Lin, C.-C., Chou, C.-H., Howng, S.-L., Hsu, C.-Y., Hwang, C.-C., Wang, C., Hsu, C.-M. and Hong, Y.-R. (2009). GSKIP, an inhibitor of GSK3beta, mediates the N-cadherin/beta-catenin pool in the differentiation of SH-SY5Y cells. *J. Cell Biochem.* **108**, 1325-1336.
Liu, J., Wang, H., Zuo, Y. and Farmer, S. R. (2006). Functional interaction between peroxisome proliferator-activated receptor gamma and beta-catenin. *Mol. Cell. Biol.* **26**, 5827-5837.
Long, L., Ormiston, M. L., Yang, X., Southwood, M., Gräf, S., Machado, R. D., Mueller, M., Kinzel, B., Yung, L. M., Wilkinson, J. M. et al. (2015). Selective enhancement of endothelial BMPR-II with BMP9 reverses pulmonary arterial hypertension. *Nat. Med.* **21**, 777-785.
Madeddu, P., Emanueli, C., Pelosi, E., Salis, M. B., Cerio, A. M., Bonanno, G., Patti, M., Stassi, G., Condorelli, G. and Peschle, C. (2004). Transplantation of low dose CD34+KDR+ cells promotes vascular and muscular regeneration in ischemic limbs. *FASEB J.* **18**, 1737-1739.

Miyake, A., Takahashi, Y., Miwa, H., Shimada, A., Konishi, M. and Itoh, N. (2009). Neucrin is a novel neural-specific secreted antagonist to canonical Wnt signaling. *Biochem. Biophys. Res. Commun.* **390**, 1051-1055.
Miyazono, K., Kamiya, Y. and Morikawa, M. (2010). Bone morphogenetic protein receptors and signal transduction. *J. Biochem.* **147**, 35-51.
Müller-Brüsselbach, S., Kömhoff, M., Rieck, M., Meissner, W., Kaddatz, K., Adamkiewicz, J., Keil, B., Klose, K. J., Moll, R., Burdick, A. D. et al. (2007). Deregulation of tumor angiogenesis and blockade of tumor growth in PPARbeta-deficient mice. *EMBO J.* **26**, 3686-3698.
Murata, T., He, S., Hangai, M., Ishibashi, T., Xi, X. P., Kim, S., Hsueh, W. A., Ryan, S. J., Law, R. E. and Hinton, D. R. (2000). Peroxisome proliferator-activated receptor-gamma ligands inhibit choroidal neovascularization. *Invest. Ophthalmol. Vis. Sci.* **41**, 2309-2317.
Nickel, N. P., Spiekerkoetter, E., Gu, M., Li, C. G., Li, H., Kaschwich, M., Diebold, I., Hennigs, J. K., Kim, K.-Y., Miyagawa, K. et al. (2015). Elafin reverses pulmonary hypertension via caveolin-1–dependent bone morphogenetic protein signaling. *Am. J. Respir. Crit. Care Med.* **191**, 1273-1286.
Nicol, C. J., Adachi, M., Akiyama, T. E. and Gonzalez, F. J. (2005). PPARgamma in endothelial cells influences high fat diet-induced hypertension. *Am. J. Hypertens.* **18**, 549-556.
Pillai, S., Kovacs, M. and Chellappan, S. (2010). Regulation of vascular endothelial growth factor receptors by Rb and E2F1: role of acetylation. *Cancer Res.* **70**, 4931-4940.
Piqueras, L., Reynolds, A. R., Hodivala-Dilke, K. M., Alfranca, A., Redondo, J. M., Hatae, T., Tanabe, T., Warner, T. D. and Bishop-Bailey, D. (2007). Activation of PPARbeta/delta induces endothelial cell proliferation and angiogenesis. *Arterioscler. Thromb. Vasc. Biol.* **27**, 63-69.
Poirier, O., Ciumas, M., Eyries, M., Montagne, K., Nadaud, S. and Soubrier, F. (2012). Inhibition of apelin expression by BMP signaling in endothelial cells. *Am. J. Physiol. Cell Physiol.* **303**, C1139-C1145.
Ricard, N., Ciais, D., Levet, S., Subileau, M., Mallet, C., Zimmers, T. A., Lee, S.-J., Bidart, M., Feige, J.-J. and Bailly, S. (2012). BMP9 and BMP10 are critical for postnatal retinal vascular remodeling. *Blood* **119**, 6162-6171.
Richardson, M. R. and Yoder, M. C. (2011). Endothelial progenitor cells: Quo Vadis? *J. Mol. Cell. Cardiol.* **50**, 266-272.
Robinson, M. D., McCarthy, D. J. and Smyth, G. K. (2010). edgeR: a Bioconductor package for differential expression analysis of digital gene expression data. *Bioinformatics* **26**, 139-140.
Rohan, R. M., Fernandez, A., Udagawa, T., Yuan, J. and D'Amato, R. J. (2000). Genetic heterogeneity of angiogenesis in mice. *FASEB J.* **14**, 871-876.
Schuch, G., Heymach, J. V., Nomi, M., Machluf, M., Force, J., Atala, A., Eder, JP, Jr., Folkman, J. and Soker, S. (2003). Endostatin inhibits the vascular endothelial growth factor-induced mobilization of endothelial progenitor cells. *Cancer Res.* **63**, 8345-8350.
Shaked, Y., Bertolini, F., Man, S., Rogers, M. S., Cervi, D., Foutz, T., Rawn, K., Voskas, D., Dumont, D. J., Ben-David, Y. et al. (2005). Genetic heterogeneity of the vasculogenic phenotype parallels angiogenesis; implications for cellular surrogate marker analysis of antiangiogenesis. *Cancer Cell* **7**, 101-111.
Shmilovich, H., Deutsch, V., Roth, A., Miller, H., Keren, G. and George, J. (2007). Circulating endothelial progenitor cells in patients with cardiac syndrome X. *Heart* **93**, 1071-1076.
Simon, D. M., Arikan, M. C., Srisuma, S., Bhattacharya, S., Tsai, L. W., Ingenito, E. P., Gonzalez, F., Shapiro, S. D. and Mariani, T. J. (2006). Epithelial cell PPAR [gamma] contributes to normal lung maturation. *FASEB J.* **20**, 1507-1509.
Spiekerkoetter, E., Tian, X., Cai, J., Hopper, R. K., Sudheendra, D., Li, C. G., El-Bizri, N., Sawada, H., Haghighat, R., Chan, R. et al. (2013). FK506 activates BMPR2, rescues endothelial dysfunction, and reverses pulmonary hypertension. *J. Clin. Invest.* **123**, 3600-3613.
Su, Y., Naser, I. B., Islam, S. M., Zhang, S., Ahmed, G., Chen, S., Shinmyo, Y., Kawakami, M., Yamamura, K.-i. and Tanaka, H. (2009). Draxin, an axon guidance protein, affects chick trunk neural crest migration. *Dev. Growth Differ.* **51**, 787-796.
Tang, Y., Harrington, A., Yang, X., Friesel, R. E. and Liaw, L. (2010). The contribution of the Tie2+ lineage to primitive and definitive hematopoietic cells. *Genesis* **48**, 563-567.
Urbich, C. and Dimmeler, S. (2004). Endothelial progenitor cells: characterization and role in vascular biology. *Circ. Res.* **95**, 343-353.
Wan, Y., Chong, L.-W. and Evans, R. M. (2007). PPAR-gamma regulates osteoclastogenesis in mice. *Nat. Med.* **13**, 1496-1503.
Wolf, D., Tseng, N., Seedorf, G., Roe, G., Abman, S. H. and Gien, J. (2014). Endothelin-1 decreases endothelial PPARgamma signaling and impairs angiogenesis after chronic intrauterine pulmonary hypertension. *Am. J. Physiol. Lung Cell. Mol. Physiol.* **306**, L361-L371.
Yasui, M., Yamamoto, H., Ngan, C. Y., Damdinsuren, B., Sugita, Y., Fukunaga, H., Gu, J., Maeda, M., Takemasa, I., Ikeda, M. et al. (2006). Antisense to cyclin D1 inhibits vascular endothelial growth factor-stimulated growth of vascular endothelial cells: implication of tumor vascularization. *Clin. Cancer Res.* **12**, 4720-4729.
Yoder, M. C. (2009). Defining human endothelial progenitor cells. *J. Thromb. Haemost.* **7** Suppl. 1, 49-52.
Zehentner, B. K., Leser, U. and Burtscher, H. (2000). BMP-2 and sonic hedgehog have contrary effects on adipocyte-like differentiation of C3H10T1/2 cells. *DNA Cell Biol.* **19**, 275-281.
Zhang, X., Gaspard, J. P. and Chung, D. C. (2001). Regulation of vascular endothelial growth factor by the Wnt and K-ras pathways in colonic neoplasia. *Cancer Res.* **61**, 6050-6054.
Zhang, M., Wang, M., Tan, X., Li, T.-F., Zhang, Y. E. and Chen, D. (2010). Smad3 prevents beta-catenin degradation and facilitates beta-catenin nuclear translocation in chondrocytes. *J. Biol. Chem.* **285**, 8703-8710.
Zilberberg, A., Yaniv, A. and Gazit, A. (2004). The low density lipoprotein receptor-1, LRP1, interacts with the human frizzled-1 (HFz1) and down-regulates the canonical Wnt signaling pathway. *J. Biol. Chem.* **279**, 17535-17542.